

Article

Synthesis, In Silico and In Vitro Evaluation for Acetylcholinesterase and BACE-1 Inhibitory Activity of Some *N*-Substituted-4-Phenothiazine-Chalcones

Thai-Son Tran ^{1,2,†}, Minh-Tri Le ^{1,3,*,†}, Thi-Cam-Vi Nguyen ⁴, The-Huan Tran ² ,
Thanh-Dao Tran ¹ and Khac-Minh Thai ^{1,*} 

¹ Department of Medicinal Chemistry, Faculty of Pharmacy, University of Medicine and Pharmacy at Ho Chi Minh City, Ho Chi Minh City 700000, Vietnam; ttson@huemed-univ.edu.vn (T.-S.T.); tranthanhdao@uphcm.edu.vn (T.-D.T.)

² Department of Pharmaceutical Chemistry, Faculty of Pharmacy, College of Medicine and Pharmacy, Hue University, Hue City 530000, Vietnam; tthuan@hueuni.edu.vn

³ School of Medicine, Vietnam National University Ho Chi Minh City, Ho Chi Minh City 700000, Vietnam

⁴ Faculty of Applied Sciences, Ton Duc Thang University, Nguyen Huu Tho St., Tan Phong Ward, Dist. 7, Ho Chi Minh City 70000, Vietnam; nguyenthicamvi@tdt.edu.vn

* Correspondence: leminhtri1099@gmail.com (M.-T.L.); thaikhacminh@ump.edu.vn (K.-M.T.); Tel.: +84-903-718-190 (M.-T.L.); +84-28-3855-2225 or +84-909-680-385 (K.-M.T.); Fax: +84-28-3822-5435 (K.-M.T.)

† T.-S.T. and M.-T.L. contributed equally to this work and are co-first authors.

Academic Editor: Diego Muñoz-Torrero

Received: 9 July 2020; Accepted: 24 August 2020; Published: 27 August 2020



Abstract: Acetylcholinesterase (AChE) and beta-secretase (BACE-1) are two attractive targets in the discovery of novel substances that could control multiple aspects of Alzheimer's disease (AD). Chalcones are the flavonoid derivatives with diverse bioactivities, including AChE and BACE-1 inhibition. In this study, a series of *N*-substituted-4-phenothiazine-chalcones was synthesized and tested for AChE and BACE-1 inhibitory activities. In silico models, including two-dimensional quantitative structure–activity relationship (2D-QSAR) for AChE and BACE-1 inhibitors, and molecular docking investigation, were developed to elucidate the experimental process. The results indicated that 13 chalcone derivatives were synthesized with relatively high yields (39–81%). The bioactivities of these substances were examined with pIC₅₀ 3.73–5.96 (AChE) and 5.20–6.81 (BACE-1). Eleven of synthesized chalcones had completely new structures. Two substances AC4 and AC12 exhibited the highest biological activities on both AChE and BACE-1. These substances could be employed for further researches. In addition to this, the present study results suggested that, by using a combination of two types of predictive models, 2D-QSAR and molecular docking, it was possible to estimate the biological activities of the prepared compounds with relatively high accuracy.

Keywords: in silico; QSAR; docking; chalcone; acetylcholinesterase inhibitor; BACE-1

1. Introduction

Alzheimer disease (AD) is an irreversible disorder resulting in dementia among the elderly [1]. This neurodegenerative ailment usually involves the impairment of the cerebral cortex through a complex process leading to the progressive cognitive decline and memory loss [2,3]. Currently, about 50 million people worldwide have been affected by the disease, thus creating a heavy burden on the health care system of many countries [4–6]. Therefore, the discovery of new drugs for AD is urgently needed.

The exact etiology of AD is currently not fully known which might be referred to as a neurological disorder caused by multiple factors, such as (i) the low concentrations of acetylcholine (ACh) in synaptic clefts; (ii) the accumulation of extracellular amyloid plaques and intracellular neurofibrillary tangles with hyperphosphorylated Tau protein; (iii) the homeostasis dysregulation of biometals; (iv) the oxidative stress [2,7–9]. The multifactorial nature of AD has transformed the paradigm of AD drug development from a single target to multiple targets, either with the multitarget-directed ligands or the cocktail therapy approach [10]. Acetylcholinesterase (AChE) and beta-secretase (BACE-1) are the two drug targets that attracted much attention among others. They are two critical enzymes in Alzheimer's pathogenesis, responsible for the defects in the cholinergic signaling pathway [11] and the formation of beta-amyloid plaques [12].

For the last few years, chalcones, belonging to flavonoid derivatives, have attracted great interest due to their diverse bioactivities, encompassing antimalarial [13,14], antimicrobial [15–27], antioxidant [28], antitumor [29–31], anti-inflammatory [32–34], analgesic [34–36], to antiulcer [37,38]. Recent studies have also indicated the abilities of chalcones in inhibiting enzymes, including alpha-glucosidase [39,40], lipoxygenase [33,41], mammalian alpha-amylase [42,43], xanthine oxidase [44], monoamine oxidase (MAO) [45–47], especially acetylcholinesterase [48–52] and beta-secretase (BACE-1) [53,54]. Therefore, the research of bioactivities of chalcone derivatives on the function of human brain, especially AChE and BACE-1 provides great promise in the discovery of new therapeutic agents for a range of neurological diseases including AD.

In the current work, a series of *N*-substituted-4-phenothiazine-chalcones was synthesized and examined for AChE and BACE-1 inhibiting effects. These compounds served as an external validation set to evaluate two-dimensional quantitative structure–activity relationship (2D-QSAR) models developed for the AChE and BACE-1 inhibitors. Molecular docking investigation was carried out to provide an insight into the molecular binding abilities of these compounds with the enzymes, through which more detailed information on structure–activity relationship (SAR) were then revealed.

2. Results and Discussion

2.1. Chemistry

Claisen–Schmidt condensation reaction [55] was applied to synthesize 13 chalcones (Figure 1) with *N*-substituted-4-acetophenothiazine and benzaldehyde derivatives as reactive agents, ethanol as solvent and sodium ethanolate as catalyst. The synthetic yields were relatively high, ranging from 39% to 81%. The structures of these substances were elucidated via IR (infrared), HR-MS (high-resolution mass spectrometry), ¹H-NMR (proton nuclear magnetic resonance), and ¹³C-NMR (carbon-13 nuclear magnetic resonance) spectra as described in the experimental section, and 11 of them were found as completely new compounds (AC2, AC4–13).

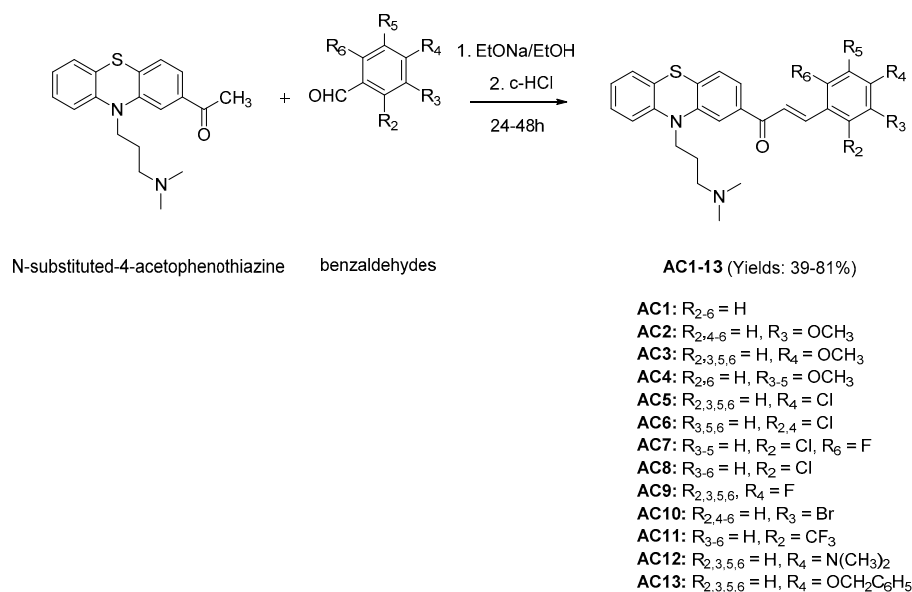


Figure 1. Claisen–Schmidt condensation reaction in chalcones synthesis. EtONa/EtOH: Sodium ethanolate in ethanol, c-HCl: concentrated hydrochloric acid.

2.2. In Vitro Assays

The results of in vitro assays on AChE and BACE-1 inhibition are indicated in Table 1. From the biological investigation, the inhibitory activities of synthesized substances against the two enzymes were obtained with pIC₅₀ values of 3.73–5.96 (IC₅₀ 186.21–1.10 μM) for AChE and 5.20–6.81 (IC₅₀ 6.34–0.16 μM) for BACE-1. Two compounds AC4 and AC12 exhibited the highest bioactivities in the synthesized substances with pIC₅₀ values of 5.44 ± 0.08 (IC₅₀ 3.63 ± 0.61 μM, AChE) and 6.81 ± 0.09 (IC₅₀ 0.16 ± 0.03 μM, BACE-1), and 5.96 ± 0.10 (IC₅₀ 1.10 ± 0.24 μM, AChE) and 6.46 ± 0.05 (IC₅₀ 0.35 ± 0.04 μM, BACE-1), respectively. In the present work, galantamine, and quercetin were used as reference substances. Galantamine is a well-known AChE inhibitor used for the treatment of cognitive decline in mild to moderate AD. Quercetin is a flavonoid reported to have an inhibitory activity against BACE-1. These two compounds have been used as references in many studies on AChE and BACE-1 inhibition. The results show that the biological activities of the positive controls in this study are comparative to the previously published values [56–58]. On the other hand, the experimental assays also specified that AC12 had a higher activity than galantamine on AChE and all the synthesized chalcones exhibited the higher inhibiting effects than quercetin on BACE-1.

Table 1. Acetylcholinesterase (AChE) and beta-secretase (BACE-1) inhibitory activities of synthesized N-substituted-4-phenothiazine-chalcones.

Compound	AChE			BACE-1		
	IC ₅₀ (μM) *	pIC ₅₀		IC ₅₀ (μM) *	pIC ₅₀	
		Observed *	Predicted		Observed *	Predicted
AC1	33.88 ± 1.45	4.47 ± 0.02	4.80	6.34 ± 0.46	5.20 ± 0.03	6.52
AC2	30.90 ± 2.10	4.51 ± 0.03	4.74	3.00 ± 0.00	5.52 ± 0.00	7.38
AC3	11.48 ± 1.29	4.94 ± 0.05	4.74	4.48 ± 0.40	5.35 ± 0.04	7.37
AC4	3.63 ± 0.61	5.44 ± 0.08	4.71	0.16 ± 0.03	6.81 ± 0.09	8.49
AC5	60.26 ± 1.84	4.22 ± 0.01	4.82	1.24 ± 0.12	5.91 ± 0.04	7.25
AC6	19.95 ± 1.57	4.70 ± 0.03	4.83	0.50 ± 0.00	6.30 ± 0.00	7.68
AC7	40.74 ± 2.48	4.39 ± 0.03	4.76	0.45 ± 0.04	6.35 ± 0.04	7.63
AC8	15.85 ± 1.08	4.80 ± 0.03	4.82	2.97 ± 0.05	5.53 ± 0.01	7.15
AC9	25.12 ± 0.83	4.60 ± 0.01	4.76	3.72 ± 0.21	5.43 ± 0.02	7.12
AC10	24.55 ± 1.09	4.61 ± 0.02	4.81	1.99 ± 0.21	5.70 ± 0.05	7.28

Table 1. Cont.

Compound	AChE			BACE-1		
	IC ₅₀ (μM) *	pIC ₅₀		IC ₅₀ (μM) *	pIC ₅₀	
		Observed *	Predicted		Observed *	Predicted
AC11	186.21 ± 4.52	3.73 ± 0.01	4.59	0.40 ± 0.00	6.40 ± 0.00	7.99
AC12	1.10 ± 0.24	5.96 ± 0.10	4.81	0.35 ± 0.04	6.46 ± 0.05	8.08
AC13	11.75 ± 0.63	4.93 ± 0.02	4.63	3.03 ± 0.21	5.52 ± 0.03	7.20
Galanthamine	1.26 ± 0.12	5.90 ± 0.04	5.14	-	-	-
Quercetin	-	-	-	9.55 ± 0.37	5.02 ± 0.02	5.24

IC₅₀: the half maximal inhibitory concentration, pIC₅₀ = -logIC₅₀. * Reported with standard deviation (SD).

2.3. Molecular Docking

The results of molecular docking study are expressed in Table 2 and in Supplementary Tables S1–S3 and Figures S1–S9. The interactions of 2 compounds with the highest pIC₅₀ (AC4 and AC12) on both enzyme AChE and BACE-1 are indicated in Figures 2 and 3. In this study, the co-crystallized complexes employed for AChE was 1DX6 (resolution: 2.30 Å) and for BACE-1 was 5HU1 (resolution: 1.50 Å). These were the complexes with high resolutions and the co-crystallized ligands were the drugs used in clinical (1DX6: galantamine) or in clinical development (5HU1: verubecestat). With this selection, the probability of docked compounds to be reached further optimization would be high. The results indicated that all studied substances were successfully docked into the binding pockets of AChE and BACE-1 with the docking scores of (−17.71)–(−27.80) kJ·mol^{−1} (AChE) and (−11.50)–(−22.51) kJ·mol^{−1} (BACE-1). A linear correlation between docking score and pIC₅₀ on AChE of synthesized chalcone derivatives were revealed (Supplementary Figure S10).

Table 2. Results of molecular docking study of the synthesized *N*-substituted-4-phenothiazine-chalcones on AChE (1DX6) and BACE-1 (5HU1).

Comp.	pIC ₅₀ (AChE)		pIC ₅₀ (BACE-1)		Docking Score (kJ·mol ^{−1}) (AChE: 1DX6)	Docking Score (kJ·mol ^{−1}) (BACE-1: 5HU1 chain A, B)
	Obs. *	Pred.	Obs. *	Pred.		
AC1	4.47 ± 0.02	4.80	5.20 ± 0.03	6.52	−25.83	−17.82; −17.69
AC2	4.51 ± 0.03	4.74	5.52 ± 0.00	7.38	−26.03	−17.22; −17.81
AC3	4.94 ± 0.05	4.74	5.35 ± 0.04	7.37	−27.67	−16.28; −15.37
AC4	5.44 ± 0.08	4.71	6.81 ± 0.09	8.49	−24.49	−16.71; −13.92
AC5	4.22 ± 0.01	4.82	5.91 ± 0.04	7.25	−17.71	−20.77; −16.87
AC6	4.70 ± 0.03	4.83	6.30 ± 0.00	7.68	−25.45	−18.79; −16.73
AC7	4.39 ± 0.03	4.76	6.35 ± 0.04	7.63	−17.94	−19.51; −16.85
AC8	4.80 ± 0.03	4.82	5.53 ± 0.01	7.15	−26.27	−20.36; −16.81
AC9	4.60 ± 0.01	4.76	5.43 ± 0.02	7.12	−27.80	−20.97; −18.06
AC10	4.61 ± 0.02	4.81	5.70 ± 0.05	7.28	−27.30	−22.51; −20.81
AC11	3.73 ± 0.01	4.59	6.40 ± 0.00	7.99	−25.33	−19.35; −16.41
AC12	5.96 ± 0.10	4.81	6.46 ± 0.05	8.08	−22.15	−18.25; −16.18
AC13	4.93 ± 0.02	4.63	5.52 ± 0.03	7.20	−23.30	−11.50; −14.09
Galantamine	5.90 ± 0.04	5.14	-	-	−28.53	-
Verubecestat	-	-	-	7.66	-	−24.95; −22.43
Quercetin	-	-	5.02 ± 0.02	5.24	-	−22.23; −23.95

Comp.: Compound, Obs.: Observed, Pred.: Predicted. * Reported with standard deviation (SD).

The docking scores of most derivatives into AChE were not significantly different (except for AC5 and AC7). In addition, the differences in the observed pIC₅₀ values could be partly explained by the analysis of the interactions between chalcone derivatives with AChE. These interactions include (i) arene–arene interactions with Trp84, Trp279, Tyr334; (ii) arene–cation interaction with Trp84; (iii) hydrogen bonding with Asp72, Glu199. These are residues of the active site-gorge of the enzyme where Trp84 and Tyr334 are exposed on the surface, particularly Asp72 on the top, Glu199 on the bottom, and Trp279 is on the entrance of the active-site gorge [59]. Eleven out of thirteen chalcone

derivatives (except for AC5 and AC11) could make a hydrogen bond to Asp72. The substituents on the benzene rings of chalcone derivatives showed no strong interaction with the enzyme. However, the presences of different groups on this ring in the chalcone structures could lead to the change in scaffold's shape as well as its interaction mode and intensity with the enzyme. There were six substances with the same interaction modes (AC3, AC4, AC6, AC9, AC10, and AC11), in which AC4 was observed with the highest activity. This could be attributed to the strongest hydrogen bond between AC4 with Asp72 (score: 64%, length: 1.52 Å) compared to the other compounds.

Compared to galantamine, all the chalcone derivatives exhibited lower bioactivities (except for AC12). This could be explained by the fact that galantamine could create an arene-cation interaction with Phe330, a strong hydrogen bond to Glu199 (score: 36%, length: 1.85 Å), and a hydrogen bond (score: 22%, length: 3.07 Å) to Ser200 (a residue in catalytic triad). AC12 had the strongest observed bioactivity among the studied substances. This can be partly explained that AC12 could yield a strong hydrogen bond to Glu199. None of the rest compounds could interact with this residue. In addition, the arene-cation interaction between AC12 and Trp84 could also lead to the increased AChE inhibitory activity of this substance in relative to the others. The interaction with Trp84 (arene-arene interaction) also made the pIC₅₀ value of AC1 equivalent to AC2 although AC1 only makes very weak hydrogen bond to Asp72 (score: 9%, length: 2.14 Å), whereas this interaction created by AC2 was very strong (score: 67%, length: 1.5 Å). Differences in the biological activity of the remaining substances can be explained by the strength of the interactions formed between those derivatives and the enzyme.

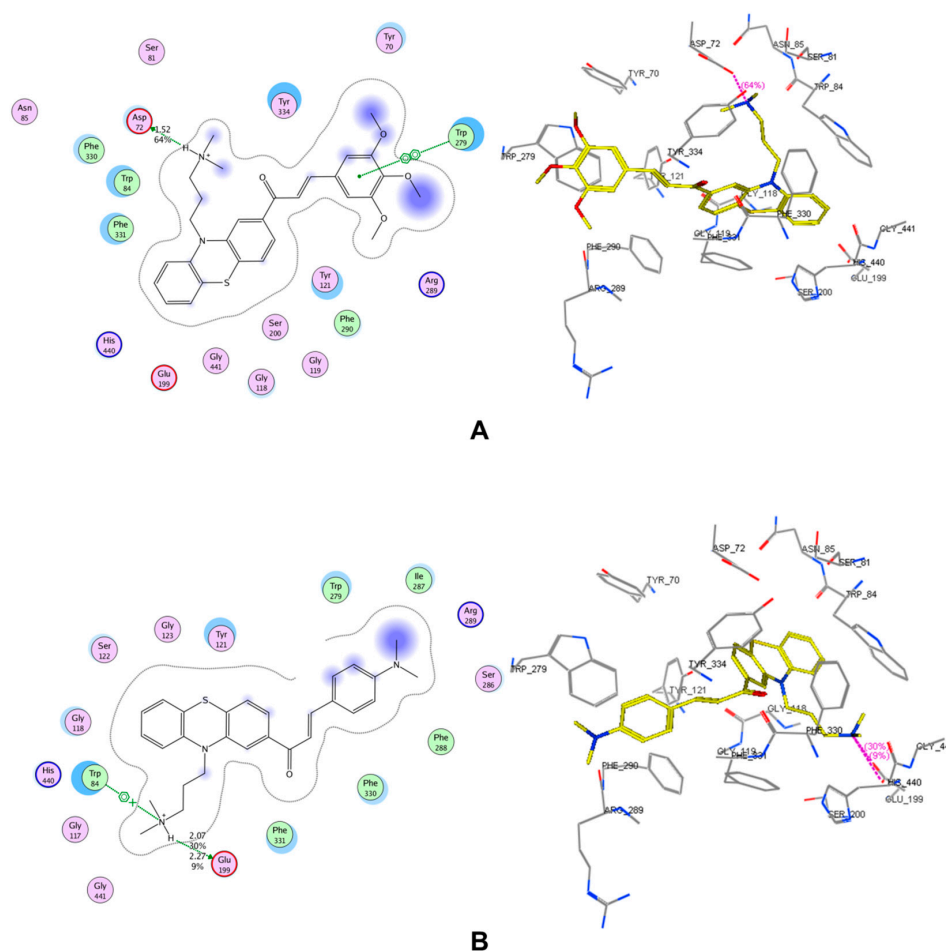


Figure 2. Interactions in the binding pocket of acetylcholinesterase (AChE, complex 1DX6) made by (A) AC4 (observed pIC₅₀: 5.44 ± 0.08), (B) AC12 (observed pIC₅₀: 5.96 ± 0.10).

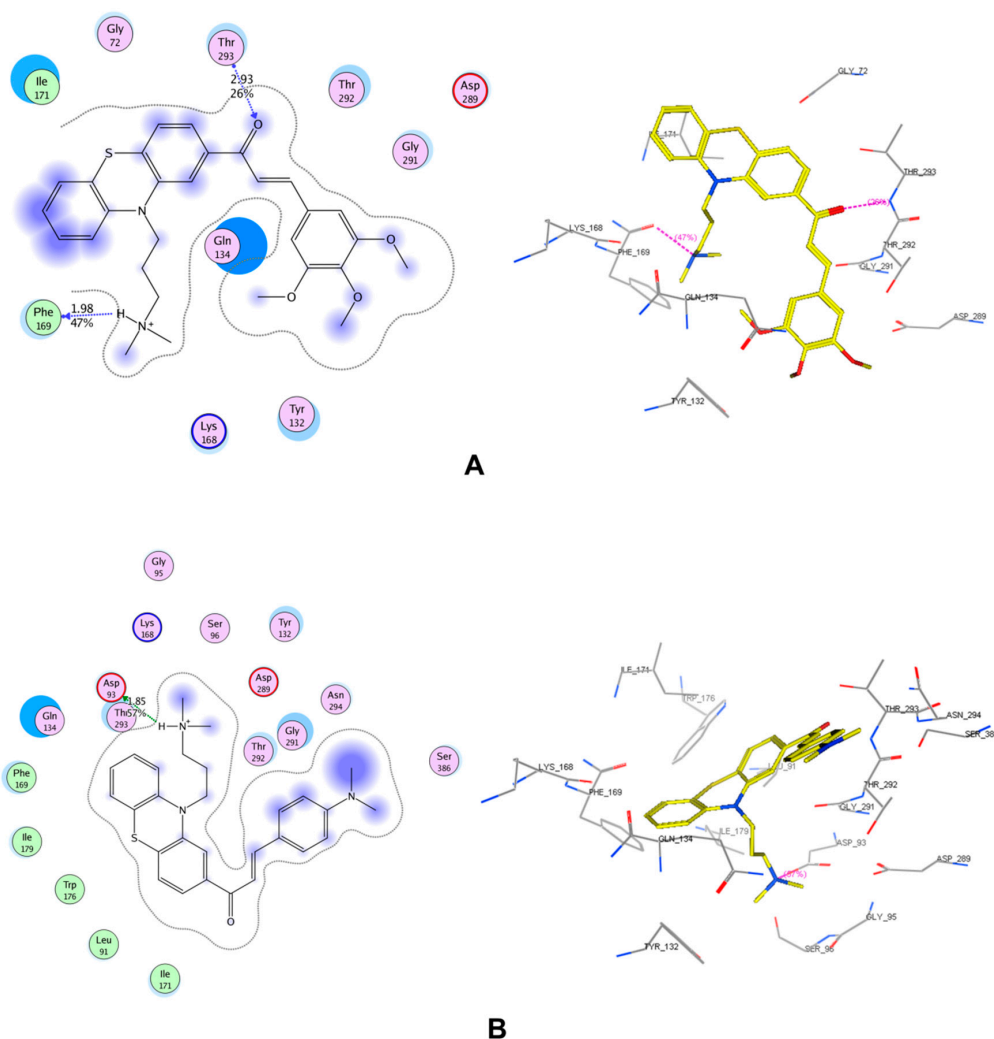


Figure 3. Interactions in the binding pocket of beta-secretase (BACE-1, complex 5HU1-chain A) made by (A) AC4 (observed pIC_{50} : 6.81 ± 0.09), (B) AC12 (observed pIC_{50} : 6.46 ± 0.05).

Molecular docking results on BACE-1 expressed that most compounds interacted with Asp93, Thr293 in the two chains of enzyme. AC1 and AC10 afforded the same interaction mode in both chains A and B of BACE-1 enzyme similar to verubecestate in this study. The others showed different interactions in the two chains. Two substances AC4 and AC12 (the most active compounds) both interacted with three residues: Asp93, Phe169 and Thr293. AC1 had a weak interaction with Asp93 in both chains of BACE-1 (chain A: hydrogen bond, score: 16%, length 2.22 Å; chain B: hydrogen bond, score: 30%, length 1.99 Å). Most of the remaining compounds formed strong hydrogen bonds with Asp93. Thus, there could be a correlation between the ability to create strong interactions with Asp93 with high BACE-1 inhibitory activity. AC13 exhibited many interactions with amino acid residues in both chains of the enzyme, except for the hydrogen bond with Asp93. The predicted and observed pIC_{50} value of this substance was as high as the others. In this study, quercetin exhibited the least bioactivity against BACE-1, but was the substance with the second highest docking score. Actually, it is not obvious that the most active compounds will always show the highest interaction energy and vice versa. Quercetin showed higher range of interaction energy due to some insignificant interactions with other elements or amino acids in the active site which have no contribution to the biological activity.

2.4. 2D-QSAR Models

The developed 2D-QSAR models for AChE and BACE-1 inhibitors were built upon the data curated from ChEMBL database [60], and reported literatures [61–72]. The data was processed appropriately according to the guidelines of OECD (Organization for Economic Co-operation and Development) for an acceptable QSAR model [73] (further details are provided in the Materials and Methods section). The validation metrics for these models are showed in Table 3. The linear regressions between the observed bioactivities and those predicted from the QSAR models are expressed in Figure 4. The data sets used to build the models and the equations used for the calculations of the validation metrics are provided in Supplementary Tables S4–S6. Selected molecular descriptors used for building 2D-QSAR models are also described in detail in Supplementary Table S7. The values of selected molecular descriptors using in predicting pIC_{50} of the synthesized chalcone derivatives are provided in Supplementary Tables S8 and S9.

Table 3. 2D-QSAR models for AChE and BACE-1 inhibitors.

AChE												
$pIC_{50} = -0.928 + (2.348 \times BCUT_SLOGP_3) - (0.150 \times reactive) - (0.004 \times PEOE_VSA + 1) - (0.005 \times PEOE_VSA - 3) - (0.002 \times SlogP_VSA2) - (0.004 \times SMR_VSA2)$												
Internal Validation					External Validation							
N	RMSE	R ²	RMSE _{LOO}	Q ² _{LOO}	N	RMSE	R ²	R ² _(PRED)	r ² _m	$\overline{r_m^2}$	Δr_m^2	CCC
50	0.18	0.70	0.22	0.57	22	0.16	0.78	0.78	0.64	0.69	0.11	0.88
BACE-1												
$pIC_{50} = 1.268 + (0.870 \times petitjean) + (6.370 \times BCUT_PEOE_1) + (3.305 \times a_ICM) - (0.478 \times chiral_u) + (0.085 \times rings) + (0.157 \times a_Nn) + (0.006 \times PEOE_VSA - 0) + (0.022 \times PEOE_VSA - 6) - (0.260 \times \log S) + (0.009 \times SlogP_VSA3) + (0.009 \times SlogP_VSA5)$												
Internal Validation					External Validation							
N	RMSE	R ²	RMSE _{LOO}	Q ² _{LOO}	N	RMSE	R ²	R ² _(PRED)	r ² _m	$\overline{r_m^2}$	Δr_m^2	CCC
150	0.37	0.80	0.40	0.77	65	0.41	0.83	0.81	0.79	0.76	0.05	0.91

N: number of compounds; RMSE (root-mean-square error), R² (squared correlation coefficient), RMSE_{LOO} (cross-validated root-mean-square error), Q²_{LOO} (cross-validated squared correlation coefficient), CCC (concordance correlation coefficient), and r²_m, $\overline{r_m^2}$, Δr_m^2 (validation metrics suggested by Roy et al. [74]).

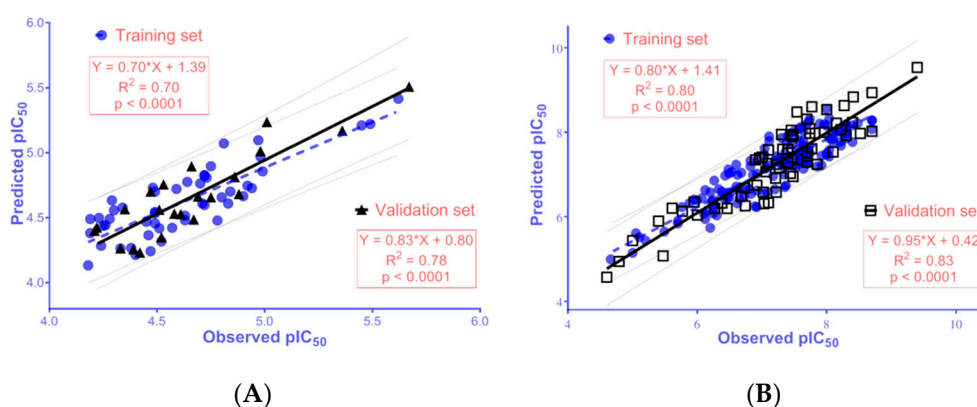


Figure 4. The linear regression between observed pIC_{50} and those predicted from the 2D-QSAR models for inhibitors of (A) AChE and (B) BACE-1.

The results exhibited that the QSAR models meet the criteria thresholds for a good model, with $R^2 = 0.70\text{--}0.83$ (>0.50), $Q^2_{LOO} = 0.57\text{--}0.77$ (>0.50), $RMSE = 0.16\text{--}0.41$ (<0.50), $RMSE_{LOO} = 0.22\text{--}0.40$ (<0.50), $R^2_{PRED} = 0.78\text{--}0.81$ (>0.50), $r_m^2 \geq 0.65$; $CCC \geq 0.85$; $\overline{r_m^2} \geq 0.5$; and $\Delta r_m^2 \leq 0.2$ [75,76].

A comparison of the statistical results obtained from the present QSAR models and the previously published works is indicated in Tables 4 and 5. Based on the statistical quality in the context of both internal and external validation criteria, the Fn-sub models reported in this study is statistically significant and sufficiently robust to predict the biological activities of new ligands.

Table 4. Comparison of this study with previous published works on 2D-QSAR model for AChE.

Source	Model	Training Set			Validation Set	
		N	R ²	Q ²	N	R ² _{PRED}
This study	PLS	55	0.70	0.57	22	0.78
Roy et al. 2018 [77]	MLR	284	0.52–0.74	0.50–0.71	142	0.50–0.63
Niraj et al. 2015 [78]	PLS	24	0.78	0.70	11	0.66

PLS: Partial least squares; MLR: Multiple linear regression; GFA: Genetic Function Approximation; N: number of compounds.

Table 5. Comparison of this study with previous published works on 2D-QSAR model for BACE1.

Source	Model	Training Set			Validation Set	
		N	R ²	Q ²	n	R ² _{PRED}
This study	PLS	150	0.80	0.77	65	0.81
Ambure et al. 2016 [79]	PLS	52	0.83	0.76	22	0.81
Ambure et al. 2016 [79]	MLR	51	0.83	0.76	22	0.80
Hossain et al. 2013 [80]	CoMFA	71	1.00	0.77	35	0.77
Hossain et al. 2013 [80]	CoMSIA	71	1.00	0.73	35	0.71
Hossain et al. 2013 [80]	PLS	71	0.94	0.79	35	0.71
Roy et al. 2018 [77]	MLR	51	0.76–0.83	0.71–0.76	23	0.75–0.91

PLS: Partial least squares; MLR: Multiple linear regression; CoMFA: Comparative molecular field analysis; CoMSIA: Comparative similarity indices analysis; LHM: Linear heuristic method; N: number of compounds.

2D-QSAR model for AChE inhibitors was developed with optimal molecular descriptors, including BCUT_SLOGP_3 (the adjacency and distance matrix), reactive (physical property), PEOE_VSA+1 and PEOE_VSA−3 (partial charge), and SlogP_VSA2 and SMR_VSA2 (subdivided surface areas). The 2D-QSAR model showed a positive correlation with BCUT_SLOGP_3, and a negative correlation with reactive, PEOE_VSA+1, PEOE_VSA−3, SlogP_VSA2, and SMR_VSA2, indicating that new ligands with high BCUT_SLOGP_3, and low reactive, PEOE_VSA+1, PEOE_VSA−3, SlogP_VSA2, SMR_VSA2 values should have higher acetylcholinesterase inhibitory activities. However, as indicated in Table 3, in the developed 2D-QSAR for AChE inhibitors, BCUT_SLOGP_3 had the highest relative importance and it played a decisive role in the predicted pIC₅₀ value. As shown in Supplementary Table S8, the studied compounds exhibited a common scaffold structure as *N*-substituted-4-phenothiazine; therefore, the BCUT_SLOGP_3 values were very close to each other, resulting in the similarity among the predicted pIC₅₀ of the chalcone derivatives. When the structure changed from chalcone to galantamine, the BCUT_SLOGP_3 value displayed a small increase whilst the predicted biological activity changed significantly, suggesting that the developed QSAR model could provide some prediction on the difference in bioactivity of substances with different scaffolds. It can be observed from Table 1 and Figure 5, the 2D-QSAR for AChE in the present work could predict quite accurately the biological activity most of synthetic chalcone derivatives, with nine out of 13 compounds displaying correlations in the predicted and observed pIC₅₀ values (R² = 0.62).

Additionally, it can be seen that the 2D-QSAR model for BACE-1 inhibitors was developed with 11 molecular descriptors, namely petitjean and BCUT_PEOE_1 (adjacency and distance matrixes), a_ICM, chiral_u, rings, and a_Nn (atom counts and bond counts), PEOE_VSA−0 and PEOE_VSA−6 (partial charges), logS (physical properties), and SlogP_VSA3 and SlogP_VSA5 (subdivided surface areas). The 2D-QSAR model reported a positive correlation between pIC₅₀ for BACE-1 inhibition with the descriptors of petitjean, BCUT_PEOE_1, a_ICM, rings, a_Nn, PEOE_VSA−0, PEOE_VSA−6,

SlogP_VSA3, SlogP_VSA5, and a negative correlation with chiral_u, logS. This thus suggested that new ligands with high petitjean, BCUT_PEOE_1, a_ICM, rings, a_Nn, PEOE_VSA-0, PEOE_VSA-6, SlogP_VSA3, SlogP_VSA5, and low chiral_u, or logS values should have higher BACE-1 inhibiting effect. The descriptor BCUT_PEOE_1 was positively correlated with biological activity; it had the highest relative importance with a decisive role to the predicted pIC₅₀ value (Table 3). The results shown in Table 1 indicate that the two substances, AC4 and AC12, had the highest observed and predicted pIC₅₀ values. This could be due to these two substances having higher BCUT_PEOE_1 values than the others (high value of BCUT_PEOE_1 was also observed in AC11, which also exhibited a high bioactivity on BACE-1). The second factor contributing to the increased pIC₅₀ values of AC4 and AC12 compared to other substances is the a_ICM descriptor which was the second most important parameter in the studied model and positively correlated with the pIC₅₀ value (Table 3). In addition, high values at other descriptors such as PEOE_VSA-0, SlogP_VSA5 (Supplementary Table S9) also contributed to the increase of pIC₅₀ of AC4 and AC12, though not much. The correlation between the QSAR predicted and observed pIC₅₀ values for BACE-1 was obtained with R² value of 0.83 (Figure 5).

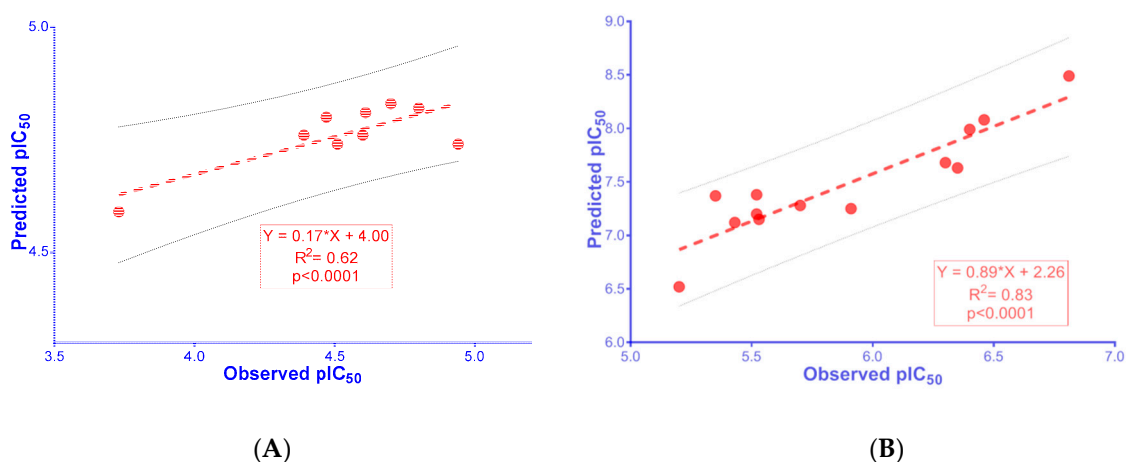


Figure 5. The linear regression between observed and predicted activities of synthesized chalcone derivatives against (A) AChE (values from AC1–3, AC6–11) and (B) BACE-1 (values from AC1–13).

3. Materials and Methods

3.1. Material and Instruments

All chemicals were obtained from commercial suppliers, and used without further purification. Melting points were determined on open capillary tubes and are uncorrected (using Gallenkamp apparatus). IR spectra were recorded on a Bruker FTIR Tensor 27 instrument. MS spectra were recorded on an Agilent 6200 Series TOF and 6500 Series Q-TOF LC/MS system. ¹H-NMR and ¹³C-NMR spectra were recorded on an AV500 Bruker (500 MHz) spectrometer. Chemical shifts were reported in parts per million (ppm) downfield relative to tetramethylsilane as an internal standard. Peak splitting patterns were abbreviated as m (multiplet), s (singlet), bs (broad singlet), d (doublet), bd (broad doublet), t (triplet), and dd (doublet of doublets).

All computation processes were performed on a computer system with the processor of Intel®Core™ i&-7700 CPU @ 3.60 Hz, 16.0 GB of RAM, the Visual Graphic Card of NVIDIA GeForce GT 1030 2GB, and the operating system of 64 bit Windows 10 (Microsoft, Redmond, WA, USA).

3.2. Chemistry

The chemical synthesis of the chalcone compounds AC1–AC13 is indicated in the Figure 1 and as follows. *N*-substituted-4-acetophenothiazine and benzaldehyde derivatives in equimolar amounts were dissolved in ethanol and cooled in ice. Sodium ethanolate was then added. The resulting

solution was stirred using an ultrasonic probe. The chemical reaction was monitored by thin layer chromatography. Final mixture was cooled and acidified by a solution of concentrated HCl to pH \approx 5–7 and left on for 24–48 h. The crude product appeared in solid or liquid. The solid was filtered, washed with cold water, and recrystallized from appropriate solvents to give the final product. With the liquid, post-reaction mixture was evaporated and purified by column chromatography with appropriate solvent systems to obtain the final product. The structures of the target compounds were elucidated by IR, MS, $^1\text{H-NMR}$, and $^{13}\text{C-NMR}$ spectra.

(*E*)-1-(10-(3-(dimethylamino)propyl)-10*H*-phenothiazin-2-yl)-3-phenylprop-2-en-1-one (AC1), Yield: 68%. Mp: Liquid at room temperature. IR ($\nu\text{ cm}^{-1}$, KBr): 2939 ($\nu_{\text{C-H sp}^3}$), 1658 ($\nu_{\text{C=O}}$), 1599 ($\nu_{\text{C=C Ar}}$), 1491 ($\nu_{\text{C=C Ar}}$), 1061 ($\nu_{\text{C-N}}$). MS: $[\text{M} + \text{H}]^+$ $m/z = 415.1814$. $^1\text{H-NMR}$ (500 MHz, MeOD, δ ppm): 7.76 (d, $J = 16$ Hz, 1H, CH=C), 7.71 (m, 2H, Ar-H), 7.66 (d, $J = 16$ Hz, 1H, CH=C), 7.61 (dd, $J_1 = 1$ Hz, $J_2 = 8$ Hz, 1H, Ar-H), 7.48 (d, 1H, Ar-H), 7.41 (m, 3H, Ar-H), 7.18 (m, 2H, Ar-H), 7.09 (dd, $J_1 = 1$ Hz, $J_2 = 7.5$ Hz, 1H, Ar-H), 6.95 (m, 2H, Ar-H), 3.94 (t, $J = 7$ Hz, 2H, N-CH₂), 2.51 (t, $J = 7.5$ Hz, 2H, N-CH₂), 2.22 (s, 6H, N-CH₃), 1.91 (m, 2H, CH₂). $^{13}\text{C-NMR}$ (125 MHz, MeOD, δ ppm): 191.1, 146.7, 146.1, 145.5, 138.4, 136.1, 133.7, 131.8, 130.1, 129.7, 128.9, 128.3, 128.2, 125.2, 124.3, 124.1, 122.8, 117.2, 115.8, 57.6, 46.1, 45.2, 25.2.

(*E*)-1-(10-(3-(dimethylamino)propyl)-10*H*-phenothiazin-2-yl)-3-(3-methoxyphenyl)prop-2-en-1-one (AC2), Yield: 43%. Mp: Liquid at room temperature. IR ($\nu\text{ cm}^{-1}$, KBr): 2970 ($\nu_{\text{C-H sp}^3}$), 1658 ($\nu_{\text{C=O}}$), 1601 ($\nu_{\text{C=C Ar}}$), 1462 ($\nu_{\text{C=C Ar}}$), 1245, ($\nu_{\text{C-O}}$), 1088 ($\nu_{\text{C-N}}$). MS: $[\text{M} + \text{H}]^+$ $m/z = 445.1977$. $^1\text{H-NMR}$ (500 MHz, MeOD, δ ppm): 7.78 (d, $J = 16$ Hz, 1H, CH=C), 7.72 (d, $J = 16$ Hz, 1H, CH=C), 7.72 (dd, $J_1 = 1.5$ Hz, $J_2 = 8.5$ Hz, 1H, Ar-H), 7.58 (d, $J = 1.5$ Hz, 1H, Ar-H), 7.35 (m, 3H, Ar-H), 7.29 (d, $J = 8$ Hz, 1H, Ar-H), 7.24 (m, 1H, Ar-H), 7.15 (dd, $J_1 = 1.5$ Hz, $J_2 = 7.5$ Hz, 1H, Ar-H), 7.05 (dd, $J_1 = 1.5$ Hz, $J_2 = 7.5$ Hz, 1H, Ar-H), 7.03 (m, 1H, Ar-H), 7.00 (m, 1H, Ar-H), 4.06 (t, $J = 7$ Hz, 2H, N-CH₂), 3.88 (s, 3H, OCH₃), 2.56 (t, $J = 7.5$ Hz, 2H, N-CH₂), 2.24 (s, 6H, N-CH₃), 2.01 (m, 2H, CH₂). $^{13}\text{C-NMR}$ (125 MHz, MeOD, δ ppm): 191.5, 146.9, 146.1, 145.8, 138.2, 137.6, 133.9, 131.0, 129.0, 128.4, 128.2, 125.4, 124.4, 124.1, 123.2, 122.4, 117.7, 117.3, 115.9, 114.6, 57.8, 55.9, 46.2, 45.3, 25.4.

(*E*)-1-(10-(3-(dimethylamino)propyl)-10*H*-phenothiazin-2-yl)-3-(4-methoxyphenyl)prop-2-en-1-one (AC3), Yield: 41%. Mp: Liquid at room temperature. IR ($\nu\text{ cm}^{-1}$, KBr): 2968 ($\nu_{\text{C-H sp}^3}$), 1655 ($\nu_{\text{C=O}}$), 1593 ($\nu_{\text{C=C Ar}}$), 1462 ($\nu_{\text{C=C Ar}}$), 1254 ($\nu_{\text{C-O}}$), 1036 ($\nu_{\text{C-N}}$). MS: $[\text{M} + \text{H}]^+$ $m/z = 445.1923$. $^1\text{H-NMR}$ (500 MHz, MeOD, δ ppm): 7.76 (d, $J = 15.5$ Hz, 1H, CH=C), 7.69 (m, 2H, Ar-H), 7.64 (dd, $J_1 = 2$ Hz, $J_2 = 8$ Hz, 1H, Ar-H), 7.56 (d, $J = 15.5$ Hz, 1H, CH=C), 7.52 (d, $J = 1.5$ Hz, 1H, Ar-H), 7.23 (m, 2H, Ar-H), 7.13 (dd, $J_1 = 1.5$ Hz, $J_2 = 7.5$ Hz, 1H, Ar-H), 7.02 (d, $J = 7.5$ Hz, 1H, Ar-H), 6.97 (m, 3H, Ar-H), 4.03 (t, $J = 7$ Hz, 2H, N-CH₂), 3.85 (s, 3H, OCH₃), 2.70 (t, $J = 7.5$ Hz, 2H, N-CH₂), 2.37 (s, 6H, N-CH₃), 2.03 (m, 2H, CH₂). $^{13}\text{C-NMR}$ (125 MHz, MeOD, δ ppm): 191.4, 146.7, 146.3, 145.6, 138.9, 133.6, 131.7, 129.0, 128.8, 128.4, 128.2, 125.5, 124.3, 124.2, 120.3, 117.3, 115.8, 115.5, 57.4, 55.9, 45.9, 44.7, 24.7.

(*E*)-1-(10-(3-(dimethylamino)propyl)-10*H*-phenothiazin-2-yl)-3-(3,4,5-trimethoxyphenyl)prop-2-en-1-one (AC4), Yield: 51%. Mp: 167–168 °C. IR ($\nu\text{ cm}^{-1}$, KBr): 2925 ($\nu_{\text{C-H sp}^3}$), 1657 ($\nu_{\text{C=O}}$), 1582 ($\nu_{\text{C=C Ar}}$), 1461 ($\nu_{\text{C=C Ar}}$), 1280 ($\nu_{\text{C-O}}$), 1124 ($\nu_{\text{C-N}}$). MS: $[\text{M} + \text{H}]^+$ $m/z = 505.2132$. $^1\text{H-NMR}$ (500 MHz, MeOD, δ ppm): 7.75 (d, $J = 15.5$ Hz, 1H, CH=C), 7.74 (dd, $J_1 = 1.5$ Hz, $J_2 = 7.5$ Hz, 1H, Ar-H), 7.67 (d, $J = 15.5$ Hz, 1H, CH=C), 7.58 (d, $J = 1.5$ Hz, 1H, Ar-H), 7.28 (d, $J = 8$ Hz, 1H, Ar-H), 7.24 (td, $J_1 = 1.5$ Hz, $J_2 = 8$ Hz, 1H, Ar-H), 7.15 (dd, $J_1 = 1.5$ Hz, $J_2 = 7.5$ Hz, 1H, Ar-H), 7.09 (s, 2H, Ar-H), 7.05 (d, $J = 7.5$ Hz, 1H, Ar-H), 6.98 (td, $J = 1$ Hz, $J = 6.5$ Hz, 1H, Ar-H), 4.06 (t, $J = 6.5$ Hz, 2H, N-CH₂), 3.92 (s, 6H, OCH₃), 3.83 (s, 3H, OCH₃), 2.28 (s, 6H, N-CH₃), 2.02 (m, 2H, CH₂). $^{13}\text{C-NMR}$ (125 MHz, MeOD, δ ppm): 191.5, 154.9, 146.9, 146.4, 145.8, 141.7, 138.7, 133.9, 132.1, 129.0, 128.4, 128.2, 125.4, 124.5, 124.2, 122.3, 117.3, 115.8, 107.4, 61.2, 57.7, 56.8, 46.1, 45.2, 25.2.

(*E*)-3-(4-chlorophenyl)-1-(10-(3-(dimethylamino)propyl)-10*H*-phenothiazin-2-yl)-3-phenylprop-2-en-1-one (AC5), Yield: 78%. Mp: Liquid at room temperature. IR (ν cm⁻¹, KBr): 2936 ($\nu_{\text{C-H sp}^3}$), 1657 ($\nu_{\text{C=O}}$), 1590 ($\nu_{\text{C=C Ar}}$), 1461 ($\nu_{\text{C=C Ar}}$), 1089 ($\nu_{\text{C-N}}$), 744 ($\nu_{\text{C-Cl}}$). MS: [M + H]⁺ m/z = 449.1451. ¹H-NMR (500 MHz, MeOD, δ ppm): 7.67 (d, J = 16 Hz, 1H, CH=C), 7.61 (m, 4H, Ar-H & CH=C), 7.44 (s, 1H, Ar-H), 7.35 (d, J = 7 Hz, 2H, Ar-H), 7.18 (t, J = 7.5 Hz, 1H, Ar-H), 7.12 (t, J = 7.5 Hz, 1H, Ar-H), 7.06 (d, J = 7.5 Hz, 1H, Ar-H), 6.93 (m, 2H, Ar-H), 3.91 (t, J = 5.5 Hz, 2H, N-CH₂), 2.48 (t, J = 7 Hz, 2H, N-CH₂), 2.20 (s, 6H, N-CH₃), 1.92 (m, 2H, CH₂). ¹³C-NMR (125 MHz, MeOD, δ ppm): 190.7, 146.7, 145.5, 144.3, 138.3, 137.4, 134.9, 133.7, 131.1, 130.2, 128.8, 128.3, 128.1, 125.1, 124.3, 124.1, 123.4, 117.2, 115.6, 57.6, 46.1, 45.2, 25.2.

(*E*)-3-(2,4-dichlorophenyl)-1-(10-(3-(dimethylamino)propyl)-10*H*-phenothiazin-2-yl)-3-phenylprop-2-en-1-one (AC6), Yield: 62%. Mp: Liquid at room temperature. IR (ν cm⁻¹, KBr): 2940 ($\nu_{\text{C-H sp}^3}$), 1658 ($\nu_{\text{C=O}}$), 1584 ($\nu_{\text{C=C Ar}}$), 1463 ($\nu_{\text{C=C Ar}}$), 1222 ($\nu_{\text{C-N}}$). MS: [M + H]⁺ m/z = 483.1054. ¹H-NMR (500 MHz, DMSO, δ ppm): 8.26 (d, J = 8.5 Hz, 1H, CH=C), 7.98 (m, 2H, Ar-H), 7.82 (dd, J_1 = 1.5 Hz, J_2 = 8 Hz, 1H), 7.78 (d, J = 2 Hz, 1H, Ar-H), 7.57 (d, J = 8 Hz, 1H, Ar-H), 7.56 (d, J = 8.5 Hz, 1H, CH=C), 7.35 (d, J = 8 Hz, 1H, Ar-H), 7.25 (td, J_1 = 1.5 Hz, J_2 = 8.5 Hz, 1H, Ar-H), 7.18 (dd, J = 1.5 Hz, J = 6.5 Hz, 1H, Ar-H), 7.08 (d, J = 7.5 Hz, 1H, Ar-H), 6.98 (td, J_1 = 1 Hz, J_2 = 6.5 Hz, 1H, Ar-H), 4.0 (t, J = 7 Hz, 2H, N-CH₂), 2.35 (t, J = 7 Hz, 2H, N-CH₂), 2.11 (s, 6H, N-(CH₃)₂), 1.83 (m, 2H, CH₂). ¹³C-NMR (125 MHz, DMSO, δ ppm): 188.1, 137.2, 136.5, 135.6, 135.1, 131.3, 131.0, 129.8, 129.5, 128.0, 127.9, 127.2, 127.1, 125.3, 123.4, 122.8, 122.3, 116.2, 114.3, 56.2, 45.2, 44.7, 24.1.

(*E*)-3-(2-chloro-6-fluorophenyl)-1-(10-(3-(dimethylamino)propyl)-10*H*-phenothiazin-2-yl)-3-phenylprop-2-en-1-one (AC7), Yield: 43%. Mp: 152–155 °C. IR (ν cm⁻¹, KBr): 2935 ($\nu_{\text{C-H sp}^3}$), 1660 ($\nu_{\text{C=O}}$), 1596 ($\nu_{\text{C=C Ar}}$), 1467 ($\nu_{\text{C=C Ar}}$), 1062 ($\nu_{\text{C-N}}$). MS: [M + H]⁺ m/z = 467.1368. ¹H-NMR (500 MHz, DMSO, δ ppm): 7.81 (d, J = 16 Hz, 1H, CH=C), 7.74 (d, J = 16 Hz, 1H, CH=C), 7.63 (dd, J_1 = 1.5 Hz, J_2 = 8 Hz, 1H, Ar-H), 7.51 (m, 3H, Ar-H), 7.40 (m, 1H, Ar-H), 7.33 (d, J = 7.5 Hz, 1H, Ar-H), 7.23 (td, J_1 = 1.5 Hz, J_2 = 8.5 Hz, 1H, Ar-H), 7.16 (dd, J_1 = 1.5 Hz, J_2 = 7.5 Hz, 1H, Ar-H), 7.06 (d, J = 8 Hz, 1H, Ar-H), 6.97 (td, J_1 = 1 Hz, J_2 = 7.5 Hz, 1H, Ar-H), 3.97 (t, J = 7 Hz, 2H, N-CH₂), 2.34 (t, J = 6.5 Hz, 2H, N-CH₂), 2.10 (s, 6H, N-CH₃), 1.82 (m, 2H, CH₂). ¹³C-NMR (125 MHz, DMSO, δ ppm): 188.4, 144.8, 143.8, 136.4, 135.0, 133.1, 132.1, 130.9, 128.8, 128.0, 127.2, 126.2, 123.0, 122.8, 122.1, 121.4, 121.3, 116.1, 115.6, 114.2, 56.2, 45.2, 44.7, 24.0.

(*E*)-3-(2-chlorophenyl)-1-(10-(3-(dimethylamino)propyl)-10*H*-phenothiazin-2-yl)-3-phenylprop-2-en-1-one (AC8), Yield: 81%. Mp: 224–227 °C. IR (ν cm⁻¹, KBr): 2957 ($\nu_{\text{C-H sp}^3}$), 1658 ($\nu_{\text{C=O}}$), 1598 ($\nu_{\text{C=C Ar}}$), 1468 ($\nu_{\text{C=C Ar}}$), 1070 ($\nu_{\text{C-N}}$). MS: [M + H]⁺ m/z = 449.1475. ¹H-NMR (500 MHz, MeOD, δ ppm): 8.23 (d, J = 15.5 Hz, 1H, CH=C), 8.03 (dd, J_1 = 1.5 Hz, J_2 = 7 Hz, 1H, Ar-H), 7.80 (d, J = 1.5 Hz, 1H, Ar-H), 7.78 (d, J = 15.5 Hz, 1H, CH=C), 7.65 (s, 1H, Ar-H), 7.52 (dd, J_1 = 1.5 Hz, J_2 = 7.5 Hz, 1H, Ar-H), 7.44 (m, 2H, Ar-H), 7.37 (d, J = 8 Hz, 1H, Ar-H), 7.30 (t, J = 7.5 Hz, 1H, Ar-H), 7.22 (d, J = 8 Hz, 1H, Ar-H), 7.12 (d, J = 8 Hz, 1H, Ar-H), 7.04 (t, J = 7.5 Hz, 1H, Ar-H), 4.19 (t, J = 6.5 Hz, 2H, N-CH₂), 3.24 (t, J = 8 Hz, 2H, N-CH₂), 2.81 (s, 6H, N-CH₃), 2.24 (m, 2H, CH₂). ¹³C-NMR (125 MHz, MeOD, δ ppm): 190.9, 146.8, 145.5, 141.3, 138.5, 136.5, 134.6, 134.2, 132.8, 131.2, 129.3, 129.2, 128.7, 128.6, 128.5, 125.9, 125.4, 124.9, 124.6, 117.5, 115.9, 56.9, 45.2, 43.8, 23.4.

(*E*)-1-(10-(3-(dimethylamino)propyl)-10*H*-phenothiazin-2-yl)-3-(4-fluorophenyl)prop-2-en-1-one (AC9), Yield: 57%. Mp: 138–140 °C. IR (ν cm⁻¹, KBr): 2931 ($\nu_{\text{C-H sp}^3}$), 1656 ($\nu_{\text{C=O}}$), 1593 ($\nu_{\text{C=C Ar}}$), 1463 ($\nu_{\text{C=C Ar}}$), 1061 ($\nu_{\text{C-N}}$). MS: [M + H]⁺ m/z = 433.1754. ¹H-NMR (500 MHz, MeOD, δ ppm): 7.79 (m, 2H, Ar-H), 7.75 (d, J = 15.5 Hz, 1H, CH=C), 7.68 (d, J = 6 Hz, 1H, Ar-H), 7.64 (d, J = 15.5 Hz, 1H, CH=C), 7.55 (s, 1H, Ar-H), 7.24 (d, J = 8.5 Hz, 1H, Ar-H), 7.22 (d, J = 8.5 Hz, 1H, Ar-H), 7.18 (d, J = 8 Hz, 1H, Ar-H), 7.16 (d, J = 8 Hz, 1H, Ar-H), 7.14 (d, J = 8.5 Hz, 1H, Ar-H), 7.04 (m, 1H, Ar-H), 6.98 (m, 1H, Ar-H), 4.04 (t, J = 6.5 Hz, 2H, N-CH₂), 2.73 (t, J = 7.5 Hz, 2H, N-CH₂), 2.39 (s, 6H, N-CH₃), 2.04 (m, 2H, CH₂). ¹³C-NMR (125 MHz, MeOD, δ ppm): 191.1, 134.0, 132.7, 132.6, 132.0, 131.9, 129.0, 128.4, 128.2, 125.5, 124.4, 124.2, 122.7, 117.3, 117.1, 116.9, 115.8, 115.4, 115.2, 56.4, 45.8, 44.7, 24.7.

(*E*)-3-(3-bromophenyl)-1-(10-(3-(dimethylamino)propyl)-10*H*-phenothiazin-2-yl)-3-phenylprop-2-en-1-one (AC10), Yield: 51%. Mp: 178–180 °C. IR (ν cm⁻¹, KBr): 2932 ($\nu_{\text{C-H sp}^3}$), 1659 ($\nu_{\text{C=O}}$), 1598 ($\nu_{\text{C=C Ar}}$), 1462 ($\nu_{\text{C=C Ar}}$), 1059 ($\nu_{\text{C-N}}$). MS: [M + H]⁺ m/z = 493.0949 and 495.1410. ¹H-NMR (500 MHz, MeOD, δ ppm): 7.94 (s, 1H, Ar-H), 7.70 (m, 4H, Ar-H & CH=C), 7.57 (m, 1H, Ar-H), 7.55 (d, J = 16 Hz, 1H, CH=C), 7.35 (m, 1H, Ar-H), 7.23 (m, 2H, Ar-H), 7.12 (dd, J_1 = 1 Hz, J_2 = 6.5 Hz, 1H), 7.02 (d, J = 8 Hz, 1H, Ar-H), 6.97 (t, J = 7.5 Hz, 1H, Ar-H), 4.02 (t, J = 6 Hz, 2H, N-CH₂), 2.52 (t, J = 7.5 Hz, 2H, N-CH₂), 2.22 (s, 6H, N-CH₃), 1.99 (m, 2H, CH₂). ¹³C-NMR (125 MHz, MeOD, δ ppm): 190.9, 146.9, 145.7, 144.1, 138.6, 138.3, 134.3, 134.0, 132.2, 131.7, 129.0, 128.6, 128.4, 128.2, 125.3, 124.5, 124.4, 124.1, 124.0, 117.3, 115.8, 57.8, 46.2, 45.3, 25.4.

(*E*)-1-(10-(3-(dimethylamino)propyl)-10*H*-phenothiazin-2-yl)-3-(2-trifluoromethyl)phenylprop-2-en-1-one (AC11), Yield: 58%. Mp: Liquid at room temperature. IR (ν cm⁻¹, KBr): 2942 ($\nu_{\text{C-H sp}^3}$), 1662 ($\nu_{\text{C=O}}$), 1592 ($\nu_{\text{C=C Ar}}$), 1463 ($\nu_{\text{C=C Ar}}$), 1123 ($\nu_{\text{C-N}}$). MS: [M + H]⁺ m/z = 483.1721. ¹H-NMR (500 MHz, MeOD, δ ppm): 8.13 (d, J = 15.5 Hz, 1H, CH=C), 8.10 (m, 1H, Ar-H), 7.77 (m, 1H, Ar-H), 7.73 (d, J = 15.5 Hz, 1H, CH=C), 7.70 (m, 2H, Ar-H), 7.59 (m, 1H, Ar-H), 7.54 (d, J = 10 Hz, 1H, Ar-H), 7.23 (m, 2H, Ar-H), 7.11 (m, 1H, Ar-H), 7.01 (t, J = 8.5 Hz, 1H, Ar-H), 6.96 (m, 1H, Ar-H), 4.00 (m, 2H, N-CH₂), 2.51 (m, 2H, N-CH₂), 2.22 (s, 3H, N-CH₃), 2.21 (s, 3H, N-CH₃), 1.96 (m, 2H, CH₂). ¹³C-NMR (125 MHz, MeOD, δ ppm): 190.5, 146.9, 145.6, 140.5, 138.1, 134.9, 134.2, 133.7, 131.2, 129.9, 129.5, 129.0, 128.4, 128.2, 127.1, 127.0, 126.7, 125.2, 124.4, 124.1, 117.3, 115.8, 57.7, 46.2, 45.3, 25.3.

(*E*)-3-(4-(dimethylamino)phenyl)-1-(10-(3-(dimethylamino)propyl)-10*H*-phenothiazin-2-yl)-3-phenylprop-2-en-1-one (AC12), Yield: 39%. Mp: Liquid at room temperature. IR (ν cm⁻¹, KBr): 2936 ($\nu_{\text{C-H sp}^3}$), 1647 ($\nu_{\text{C=O}}$), 1572 ($\nu_{\text{C=C Ar}}$), 1459 ($\nu_{\text{C=C Ar}}$), 1168 ($\nu_{\text{C-N}}$). MS: [M + H]⁺ m/z = 458.2298. ¹H-NMR (500 MHz, MeOD, δ ppm): 7.76 (d, J = 15.5 Hz, 1H, CH=C), 7.60 (m, 3H, Ar-H), 7.51 (s, 1H, Ar-H), 7.43 (d, J = 15.5 Hz, 1H, CH=C), 7.22 (d, J = 8 Hz, 1H, Ar-H), 7.20 (d, J = 8 Hz, 1H, Ar-H), 7.11 (d, J = 7 Hz, 1H, Ar-H), 6.99 (d, J = 8 Hz, 1H, Ar-H), 6.95 (t, J = 7.5 Hz, 1H, Ar-H), 6.72 (d, J = 9 Hz, 2H, Ar-H), 3.98 (t, J = 6.5 Hz, 2H, N-CH₂), 3.01 (s, 6H, N-CH₃), 2.52 (t, J = 7.5 Hz, 2H, N-CH₂), 2.22 (s, 6H, N-CH₃), 1.96 (m, 2H, CH₂). ¹³C-NMR (125 MHz, MeOD, δ ppm): 191.5, 153.9, 147.8, 146.7, 145.8, 139.4, 132.9, 131.9, 128.9, 128.4, 128.1, 125.4, 124.1, 123.7, 117.3, 117.0, 115.8, 113.0, 57.7, 46.1, 45.3, 40.2, 25.3.

(*E*)-3-(4-(benzyloxy)phenyl)-1-(10-(3-(dimethylamino)propyl)-10*H*-phenothiazin-2-yl)-3-phenylprop-2-en-1-one (AC13), Yield: 40%. Mp: 183–185 °C. IR (ν cm⁻¹, KBr): 2936 ($\nu_{\text{C-H sp}^3}$), 1655 ($\nu_{\text{C=O}}$), 1592 ($\nu_{\text{C=C Ar}}$), 1459 ($\nu_{\text{C=C Ar}}$), 1247 ($\nu_{\text{C-O}}$), 1060 ($\nu_{\text{C-N}}$). MS: [M + H]⁺ m/z = 521.2243. ¹H-NMR (500 MHz, MeOD+DMSO, δ ppm): 7.80 (d, J = 15.5 Hz, 1H, CH=C), 7.79 (m, 2H, Ar-H), 7.74 (dd, J_1 = 1.5 Hz, J_2 = 8 Hz, 1H, Ar-H), 7.67 (d, J = 15.5 Hz, 1H, CH=C), 7.62 (d, J = 1.5 Hz, 1H, Ar-H), 7.51 (d, J = 7 Hz, 2H, Ar-H), 7.44 (m, 2H, Ar-H), 7.38 (m, 1H, Ar-H), 7.33 (d, J = 7.5 Hz, 1H, Ar-H), 7.28 (td, J_1 = 1.5 Hz, J_2 = 8.5 Hz, 1H, Ar-H), 7.20 (dd, J = 2 Hz, J = 7.5 Hz, 1H), 7.13 (m, 2H, Ar-H), 7.10 (d, J = 8 Hz, 1H, Ar-H), 7.00 (td, J_1 = 1.5 Hz, J_2 = 8 Hz, 1H, Ar-H), 5.22 (s, 2H, OCH₂), 4.10 (t, J = 7 Hz, 2H, N-CH₂), 2.55 (t, J = 7 Hz, 2H, N-CH₂), 2.24 (s, 6H, N-CH₃), 2.20 (m, 2H, CH₂). ¹³C-NMR (125 MHz, MeOD + DMSO, δ ppm): 190.8, 162.4, 146.8, 145.9, 145.8, 138.9, 138.3, 133.1, 131.9, 129.2, 129.1, 128.8, 128.4, 128.2, 125.1, 124.3, 124.2, 120.7, 117.4, 116.6, 115.9, 71.1, 57.8, 46.2, 45.6, 25.5.

3.3. Acetylcholinesterase Inhibitory Activity Assay

AChE inhibitory activities of chalcones were determined by Ellman's colourimetric method using purified acetylcholinesterase from electric eel (Type VI) and acetylthiocholine iodide (ATCI) as a substrate and galantamine as a reference. The assay was performed in 96-well microtiter plates in the same condition for both chalcones and control substance. 25 μ L of 100 mM sodium phosphate buffer pH 8, 25 μ L of sample and 25 μ L acetylcholinesterase solutions containing 0.54 U/mL were mixed in each well of the plate and allowed to incubate for 15 min at 25 °C. Subsequently, 25 μ L of a solution of ATCI (15 mM, dissolved in water) and 125 μ L of 3 mM DTNB (5,5'-dithio-bis-nitro benzoic acid) were added. The absorbance at 405 nm was recorded during the first 5 min of the reaction. A control reaction, which was considered to have 100% activity, was carried out using the same volume of

methanol/water instead of tested solutions. All samples and the positive control (galantamine) were assayed in triplicate. Percentages (%) of AChE inhibitions of tested compounds were calculated from the absorbance values as indicated in Equation (1):

$$\% I = [(A_{0E} - A_0) - (A_c - A_{0C})]/(A_{0E} - A_0) \quad (1)$$

where I is the percent inhibition of acetylcholinesterase; A_{0E} is the absorbance value of the control blank sample with enzyme; A_0 is the absorbance value of blank sample; A_c is the absorbance value of the tested sample; A_{0C} is the absorbance value of blank test sample.

The content of each sample was indicated in Table 6.

Table 6. The content of each sample in AChE in vitro assay.

Samples	ATCI	DTNB	Buffer	Chalcone	AChE
Control blank sample with enzyme (A_{0E})	+	+	+	–	+
Blank sample (A_0)	+	+	+	–	–
Tested sample (A_c)	+	+	+	+	+
Blank test sample (A_{0C})	+	+	+	+	–

+: present; –: absent.

Linear recurrent equations indicating the correlation between common logarithm of the concentration of investigated compounds (μM) and their percentages of AChE inhibition (%) were built, from which the IC_{50} values (concentration that inhibits 50% AChE activity) of studied chalcones were extrapolated. The method was as described earlier [81].

3.4. β -secretase Inhibitory Activity Assay

β -secretase (BACE-1) Activity Detection Kit (Fluorescent) was purchased from Sigma–Aldrich and used to determine the effect of the synthesized chalcones on β -secretase activity. The assay was carried out according to the manufacturer's protocol. The enzyme solution (0.3 units/uL, 2 μL) was reacted with the 50 μM of the substrate (7-methoxycumarin- 4-acetyl-(Asn670, Lue671)-amyloid β /A4 precursor protein 770 fragment 667–676-(2,4-dinitrophenyl))Lys-Arg-Arg amide trifluoroacetate salt and sulfated polysaccharide samples (2–5 mg/mL) in a fluorescence assay buffer in different wells. Baseline readings were measure immediately on a Hitachi F-7000 (excitation: 320 nm; emission: 405 nm) fluorescence spectrophotometer and repeated after 2 h incubation at 37 °C. Quercetin was used as the positive control. The method was as described earlier [82,83].

3.5. Building 2D-QSAR Model

3.5.1. Data Collection and Ligand Preparation

The dataset of AChE inhibitors was obtained from ChEMBL database [60], and the BACE-1 inhibitor database was collected from reported literatures [61–72]. Initial processing of input data was then carried out, including rejecting substances with similar structures (use Cluster codes tool in MOE 2008.10 [84]), retaining compounds with the same bioassay method, and correcting IC_{50} appropriately. A total of 72 derivatives, with AChE inhibitory activities which were determined using Ellman's method on the enzyme of *Electrophorus electricus* and galantamine as a reference, were finally obtained. The total number of BACE-1 inhibitors with the same FRET (Fluorescence Resonance Energy Transfer) test method was 215 (Supplementary Tables S4 and S5). IC_{50} values were then converted into pIC_{50} for convenient calculations. The structures were built directly in Sybyl X 2.0 [85]. These final datasets were used to build 2D-QSAR models with optimal molecular descriptors.

3.5.2. Molecular Descriptors Calculation and Processing

One hundred and eighty-four 2D molecular descriptors were calculated in MOE 2008.10, and then processed to eliminate redundant or irrelevant features for improving model quality and reducing computational time consumption [86]. Firstly, the molecular descriptors were filtered and removed useless or correlated attributes using RapidMiner 5.3.008 [87]. Subsequently, they were processed further by BestFirst search method of Weka 3.8 [88] to figure out parameters having the optimal values with 10-fold cross validation. Selected molecular descriptors used for building 2D-QSAR models in this study are described in detail in the Supplementary Table S7.

3.5.3. Database Division into Training Set and Validation Set

The database was divided into training set and validation set in a ratio of 70% to 30% using randomization method. The Rand function in MOE 2008.10 was used to split randomly the database of compounds, each of which was assigned a random number between 0 and 1.

3.5.4. Model Building and Validation

2D-QSAR model was built using the partial least square (PLS) method and then validated by the values of RMSE (root-mean-square error), R^2 (squared correlation coefficient), $RMSE_{LOO}$ (cross-validated root-mean-square error), Q^2_{LOO} (cross-validated squared correlation coefficient), and more widely used metrics r_m^2 , $r_m'^2$, $\overline{r_m^2}$, Δr_m^2 ; R^2_{PRED} , or CCC (concordance correlation coefficient) [89]. The equation used for calculation of these metrics are provided in the Supplementary Table S6.

3.6. Molecular Docking Procedure

Docking was firstly performed on 3 conformations of co-crystallized ligand to validate the procedure. The RMSD (Root-Mean-Square Deviation) value between re-docked conformations and the original bound ligand in the co-crystallized complex which was $\leq 1.5 \text{ \AA}$ would indicate the reliability of the binding ability prediction of new ligands [90]. Docking process was performed using complexes 1DX6 of AChE (resolution 2.3 \AA) and 5HU1 (resolution 1.5 \AA) of BACE-1 downloaded from Protein Data Bank [91] and FlexX program in BioSolveIT LeadIt [92] with default settings. This program applied the flexible-based docking methodology, in which the ligand was treated as a flexible component and the protein was kept rigid during docking process. FlexX used an incremental construction algorithm for the search of ligand conformations. The base fragment was first placed into the active site by matching interaction geometries between the ligand and protein. Then, the remains were gradually built-up in conformity with a set of predefined rotatable torsion angles to account for ligand flexibility. The FlexX utilised empirical scoring functions to score and rank the docking poses [93,94].

The interactions between chalcone molecules and their target were rendered and analyzed in MOE 2008.10 program (hydrogen bonds, π - π interactions, cation- π interactions, ionic interactions). Moreover, van der Waals surface interactions were detected by the contact of hydrophilic and lipophilic surfaces of the ligands with those of binding points.

4. Conclusions

In this study, 13 *N*-substituted-4-phenothiazine-chalcone derivatives were synthesized and tested for AChE and BACE-1 inhibition with the pIC_{50} values of 3.73–5.96 (AChE) and 5.20–6.81 (BACE-1). Two 2D-QSAR models were built from curated data and validated through evaluation metrics. These models could be used to predict the bioactivities of chemical compounds with high reliabilities. The synthesized substances were considered as an external validation set to evaluate the developed 2D-QSAR model for AChE and BACE-1 inhibitors with relatively high correlations between the observed and estimated bioactivities ($R^2 = 0.62$ for AChE and $R^2 = 0.83$ for BACE-1). Eleven of the synthesized derivatives were newly discovered (AC2, AC4–13). The molecular docking model developed in the present work could be used to explain the difference in the observed biological

activity compared to the predicted value as the 2D-QSAR models could not clearly interpreted. Thus, the combination of 2D and 3D models, between ligand- and structure-based drug designs, could allow for the prediction of the biological activities of chemical substances more accurately. Among the studied *N*-substituted-4-phenothiazine-chalcones, AC4 and AC12 were two derivatives with the strongest inhibitory activities against both AChE and BACE-1. These substances could be used in further studies. In addition, many substances need to be synthesized and tested for AChE and BACE-1 inhibitory activities to further validate the performance of the developed 2D-QSAR models.

Supplementary Materials: The following are available online. Table S1. Results of re-docking (RMSD in Å), Table S2: Docking results and ligand interaction (Co-crystallized 1DX6), Table S3. Docking results and ligand interaction (Co-crystallized 5HU1 chain A and B), Table S4. Dataset of 72 compounds used in the building of 2D-QSAR model for AChE inhibitors, Table S5. Dataset of 215 compounds used in the building of 2D-QSAR model for BACE-1 inhibitors, Table S6. Equations for calculation of 2D-QSAR validation metrics, Table S7. Selected descriptors used for building 2D-QSAR models, Table S8. Values of selected descriptors used in prediction of pIC₅₀ of the synthesized chalcone derivatives (AChE), Table S9. Values of selected descriptors used in prediction of pIC₅₀ of the synthesized chalcone derivatives (BACE-1), Table S10. Spectra of synthesized chalcone derivatives, Figure S1. Interactions of co-crystallized ligand in the protein complex 1DX6 (2D), Figure S2. Interactions of co-crystallized ligand in the protein complex 1DX6 (3D), Figure S3. Alignment of re-dock ligands with the native one in the binding pocket of of 1DX6, Figure S4. Interactions of co-crystallized ligand in the protein complex 5HU1-chain A (2D), Figure S5. Interactions of co-crystallized ligand in the protein complex 5HU1-chain A (3D), Figure S6. Alignment of re-dock ligands with the native one in the binding pocket of of 5HU1-chain A, Figure S7. Interactions of co-crystallized ligand in the protein complex 5HU1-chain B (2D), Figure S8. Interactions of co-crystallized ligand in the protein complex 5HU1-chain B (3D), Figure S9. Alignment of re-dock ligands with the native one in the binding pocket of of 5HU1-chain B, Figure S10. The linear regression between docking score and pIC₅₀ on AChE of synthesized chalcone derivatives (A. observed values from AC1–3 and AC5–10, B. predicted values from AC1, AC4, AC6, AC8, AC10, AC13).

Author Contributions: Conceptualization, T.-D.T. and K.-M.T.; Data curation, T.-S.T. and K.-M.T.; Formal analysis, T.-S.T., M.-T.L., and K.-M.T.; Funding acquisition, K.-M.T.; Investigation, T.-S.T., M.-T.L., T.-C.-V.N., T.-H.T., T.-H.T., and K.-M.T.; Methodology, T.-S.T., M.-T.L., T.-H.T., and K.-M.T.; Resources, M.-T.L., T.-H.T., and K.-M.T.; Software, T.-S.T., T.-C.-V.N., T.-H.T., and K.-M.T.; Supervision, T.-D.T. and K.-M.T.; Validation, T.-S.T., M.-T.L., T.-H.T., T.-H.T., and K.-M.T.; Visualization, T.-S.T. and K.-M.T.; Writing—original draft, T.-S.T., M.-T.L., T.-H.T., T.-H.T., and K.-M.T.; Writing—review & editing, T.-S.T., M.-T.L., T.-C.-V.N., T.-H.T., T.-H.T., and K.-M.T. All authors have read and agreed to the published version of the manuscript.

Funding: This research is funded by Vietnam National Foundation for Science and Technology Development (NAFOSTED) under grant number 106-YS.05-2015.31 to Khac-Minh Thai.

Conflicts of Interest: The authors declare no conflict of interest.

References

1. Kim, M.; Park, H.E.; Lee, S.-H.; Han, K.; Lee, J.H. Increased risk of Alzheimer's disease in patients with psoriasis: A nationwide population-based cohort study. *Sci. Rep.* **2020**, *10*, 6454. [[CrossRef](#)]
2. Ringman, J.M. Update on Alzheimer's and the Dementias: Introduction. *Neurol. Clin.* **2017**, *35*, 171–174. [[CrossRef](#)] [[PubMed](#)]
3. Graham, W.V.; Bonito-Oliva, A.; Sakmar, T.P. Update on Alzheimer's Disease Therapy and Prevention Strategies. *Annu. Rev. Med.* **2017**, *68*, 413–430. [[CrossRef](#)] [[PubMed](#)]
4. Guo, S.; Getsios, D.; Revankar, N.; Xu, P.; Thompson, G.; Bobula, J.; Lacey, L.; Gaudig, M. Evaluating disease-modifying agents: A simulation framework for Alzheimer's disease. *Pharmacoeconomics* **2014**, *32*, 1129–1139. [[CrossRef](#)] [[PubMed](#)]
5. Alzheimer's Association 2015. Alzheimer's disease facts and figures. *Alzheimers Dement.* **2015**, *11*, 332–384.
6. Lalut, J.; Payan, H.; Davis, A.; Lecoutey, C.; Legay, R.; Santos, J.S.-D.O.; Claeysen, S.; Dallemagne, P.; Rochais, C. Rational design of novel benzisoxazole derivatives with acetylcholinesterase inhibitory and serotonergic 5-HT₄ receptors activities for the treatment of Alzheimer's disease. *Sci. Rep.* **2020**, *10*, 3014. [[CrossRef](#)]
7. Blazer, L.L.; Neubig, R.R. Small molecule protein-protein interaction inhibitors as CNS therapeutic agents: Current progress and future hurdles. *Neuropsychopharmacology* **2009**, *34*, 126–141. [[CrossRef](#)]
8. Querfurth, H.W.; LaFerla, F.M. Alzheimer's disease. *N. Engl. J. Med.* **2010**, *362*, 329–344. [[CrossRef](#)]

9. Tumiatti, V.; Minarini, A.; Bolognesi, M.L.; Milelli, A.; Rosini, M.; Melchiorre, C. Tacrine derivatives and Alzheimer's disease. *Curr. Med. Chem.* **2010**, *17*, 1825–1838. [[CrossRef](#)]
10. Gong, C.X.; Liu, F.; Iqbal, K. Multifactorial Hypothesis and Multi-Targets for Alzheimer's Disease. *J. Alzheimers Dis.* **2018**, *64*, S107–S117. [[CrossRef](#)]
11. Rees, T.M.; Brimijoin, S. The role of acetylcholinesterase in the pathogenesis of Alzheimer's disease. *Drugs Today* **2003**, *39*, 75–83. [[CrossRef](#)] [[PubMed](#)]
12. Vassar, R. BACE1: The beta-secretase enzyme in Alzheimer's disease. *J. Mol. Neurosci.* **2004**, *23*, 105–114. [[CrossRef](#)]
13. Kumar, D.; Kumar, M.; Kumar, A.; Singh, S.K. Chalcone and curcumin derivatives: A way ahead for malarial treatment. *Mini Rev. Med. Chem.* **2013**, *13*, 2116–2133. [[CrossRef](#)] [[PubMed](#)]
14. Singh, P.; Anand, A.; Kumar, V. Recent developments in biological activities of chalcones: A mini review. *Eur. J. Med. Chem.* **2014**, *85*, 758–777. [[CrossRef](#)]
15. Lunardi, F.; Guzela, M.; Rodrigues, A.T.; Corrêa, R.; Eger-Mangrich, I.; Steindel, M.; Grisard, E.C.; Assreuy, J.; Calixto, J.B.; Santos, A.R.S. Trypanocidal and Leishmanicidal Properties of Substitution-Containing Chalcones. *Antimicrob. Agents Chemother.* **2003**, *47*, 1449–1451. [[CrossRef](#)]
16. De Mello, T.F.; Cardoso, B.M.; Lopes, S.N.; Bitencourt, H.R.; Voltarelli, E.M.; Hernandez, L.; Aristides, S.M.; Lonardon, M.V.; Silveira, T.G. Activity of synthetic chalcones in hamsters experimentally infected with *Leishmania (Viannia) braziliensis*. *Parasitol. Res.* **2015**, *114*, 3587–3600. [[CrossRef](#)]
17. Passalacqua, T.G.; Dutra, L.A.; de Almeida, L.; Velasquez, A.M.; Torres, F.A.; Yamasaki, P.R.; dos Santos, M.B.; Regasini, L.O.; Michels, P.A.; Bolzani, V.D.S.; et al. Synthesis and evaluation of novel prenylated chalcone derivatives as anti-leishmanial and anti-trypanosomal compounds. *Bioorg. Med. Chem. Lett.* **2015**, *25*, 3342–3345. [[CrossRef](#)]
18. Shakhathreh, M.A.; Al-Smadi, M.L.; Khabour, O.F.; Shuaibu, F.A.; Hussein, E.I.; Alzoubi, K.H. Study of the antibacterial and antifungal activities of synthetic benzyl bromides, ketones, and corresponding chalcone derivatives. *Drug Des. Dev. Ther.* **2016**, *10*, 3653–3660. [[CrossRef](#)]
19. Wei, Z.Y.; Chi, K.Q.; Yu, Z.K.; Liu, H.Y.; Sun, L.P.; Zheng, C.J.; Piao, H.R. Synthesis and biological evaluation of chalcone derivatives containing aminoguanidine or acylhydrazone moieties. *Bioorg. Med. Chem. Lett.* **2016**, *26*, 5920–5925. [[CrossRef](#)]
20. Evranos-Aksoz, B.; Onurdag, F.K.; Ozgacar, S.O. Antibacterial, antifungal and antimycobacterial activities of some pyrazoline, hydrazone and chalcone derivatives. *Zeitschrift für Naturforschung C* **2015**, *70*, 183–189. [[CrossRef](#)]
21. Tran, T.D.; Do, T.H.; Tran, N.C.; Ngo, T.D.; Huynh, T.N.; Tran, C.D.; Thai, K.M. Synthesis and anti Methicillin resistant *Staphylococcus aureus* activity of substituted chalcones alone and in combination with non-beta-lactam antibiotics. *Bioorg. Med. Chem. Lett.* **2012**, *22*, 4555–4560. [[CrossRef](#)]
22. Yin, B.T.; Yan, C.Y.; Peng, X.M.; Zhang, S.L.; Rasheed, S.; Geng, R.X.; Zhou, C.H. Synthesis and biological evaluation of alpha-triazolyl chalcones as a new type of potential antimicrobial agents and their interaction with calf thymus DNA and human serum albumin. *Eur. J. Med. Chem.* **2014**, *71*, 148–159. [[CrossRef](#)] [[PubMed](#)]
23. Wang, Y.H.; Dong, H.H.; Zhao, F.; Wang, J.; Yan, F.; Jiang, Y.Y.; Jin, Y.S. The synthesis and synergistic antifungal effects of chalcones against drug resistant *Candida albicans*. *Bioorg. Med. Chem. Lett.* **2016**, *26*, 3098–3102. [[CrossRef](#)] [[PubMed](#)]
24. Lahtchev, K.L.; Batovska, D.I.; Parushev, S.P.; Ubivovk, V.M.; Sibirny, A.A. Antifungal activity of chalcones: A mechanistic study using various yeast strains. *Eur. J. Med. Chem.* **2008**, *43*, 2220–2228. [[CrossRef](#)] [[PubMed](#)]
25. Mateeva, N.; Eyunni, S.V.K.; Redda, K.K.; Ononuju, U.; Hansberry, T.D., II; Aikens, C.; Nag, A. Functional evaluation of synthetic flavonoids and chalcones for potential antiviral and anticancer properties. *Bioorg. Med. Chem. Lett.* **2017**, *27*, 2350–2356. [[CrossRef](#)] [[PubMed](#)]
26. Patil, S.A.; Patil, V.; Patil, R.; Beaman, K.; Patil, S.A. Identification of novel 5,6-dimethoxyindan-1-one derivatives as antiviral agents. *Med. Chem. Med. Chem.* **2017**, *13*, 787–795. [[CrossRef](#)]
27. Lee, J.S.; Bukhari, S.N.; Fauzi, N.M. Effects of chalcone derivatives on players of the immune system. *Drug Des. Dev. Ther.* **2015**, *9*, 4761–4778. [[CrossRef](#)]
28. Sivakumar, P.M.; Prabhakar, P.K.; Doble, M. Synthesis, antioxidant evaluation, and quantitative structure–activity relationship studies of chalcones. *Med. Chem. Res.* **2011**, *20*, 482–492. [[CrossRef](#)]

29. Yamali, C.; Gul, H.I.; Ozgun, D.O.; Hiroshi, S.S.; Umemura, N.; Kazaz, C.; Gul, M. Synthesis and Cytotoxic Activities of Difluoro-Dimethoxy Chalcones. *Anticancer Agents Med. Chem.* **2017**, *17*. [[CrossRef](#)]
30. Sakagami, H.; Masuda, Y.; Tomomura, M.; Yokose, S.; Uesawa, Y.; Ikezoe, N.; Asahara, D.; Takao, K.; Kanamoto, T.; Terakubo, S.; et al. Quantitative Structure-Cytotoxicity Relationship of Chalcones. *Anticancer Res.* **2017**, *37*, 1091–1098. [[CrossRef](#)]
31. Echeverria, C.; Santibanez, J.F.; Donoso-Tauda, O.; Escobar, C.A.; Ramirez-Tagle, R. Structural antitumoral activity relationships of synthetic chalcones. *Int. J. Mol. Sci.* **2009**, *10*, 221–231. [[CrossRef](#)] [[PubMed](#)]
32. Ozdemir, A.; Altintop, M.D.; Turan-Zitouni, G.; Ciftci, G.A.; Ertorun, I.; Alatas, O.; Kaplancikli, Z.A. Synthesis and evaluation of new indole-based chalcones as potential antiinflammatory agents. *Eur. J. Med. Chem.* **2015**, *89*, 304–309. [[CrossRef](#)] [[PubMed](#)]
33. Jantan, I.; Bukhari, S.N.A.; Adekoya, O.A.; Sylte, I. Studies of synthetic chalcone derivatives as potential inhibitors of secretory phospholipase A(2), cyclooxygenases, lipoxygenase and pro-inflammatory cytokines. *Drug Des. Dev. Ther.* **2014**, *8*, 1405–1418. [[CrossRef](#)] [[PubMed](#)]
34. Abdellatif, K.R.; Elshemy, H.A.; Salama, S.A.; Omar, H.A. Synthesis, characterization and biological evaluation of novel 4'-fluoro-2'-hydroxy-chalcone derivatives as antioxidant, anti-inflammatory and analgesic agents. *J. Enzym. Inhib. Med. Chem.* **2015**, *30*, 484–491. [[CrossRef](#)]
35. Heidari, M.R.; Foroumadi, A.; Noroozi, H.; Samzadeh-Kermani, A.; Azimzadeh, B.S. Study of the anti-inflammatory and analgesic effects of novel rigid benzofuran-3, 4-dihydroxy chalcone by formalin, hot-plate and carrageenan tests in mice. *Pak. J. Pharm Sci.* **2009**, *22*, 395–401.
36. Ismail, N.I.; Ming-Tatt, L.; Lajis, N.; Akhtar, M.N.; Akira, A.; Perimal, E.K.; Israf, D.A.; Sulaiman, M.R. Antinociceptive Effect of 3-(2,3-Dimethoxyphenyl)-1-(5-methylfuran-2-yl)prop-2-en-1-one in Mice Models of Induced Nociception. *Molecules* **2016**, *21*, 1077. [[CrossRef](#)]
37. Dhiyaaldeen, S.M.; Amin, Z.A.; Darvish, P.H.; Mustafa, I.F.; Jamil, M.M.; Rouhollahi, E.; Abdulla, M.A. Protective effects of (1-(4-hydroxy-phenyl)-3-m-tolyl-propenone chalcone in indomethacin-induced gastric erosive damage in rats. *BMC Vet. Res.* **2014**, *10*, 961. [[CrossRef](#)]
38. Sashidhara, K.V.; Avula, S.R.; Mishra, V.; Palnati, G.R.; Singh, L.R.; Singh, N.; Chhonker, Y.S.; Swami, P.; Bhatta, R.S.; Palit, G. Identification of quinoline-chalcone hybrids as potential antiulcer agents. *Eur. J. Med. Chem.* **2015**, *89*, 638–653. [[CrossRef](#)]
39. Ansari, F.L.; Umbreen, S.; Hussain, L.; Makhmoor, T.; Nawaz, S.A.; Lodhi, M.A.; Khan, S.N.; Shaheen, F.; Choudhary, M.I. Syntheses and biological activities of chalcone and 1,5-benzothiazepine derivatives: Promising new free-radical scavengers, and esterase, urease, and alpha-glucosidase inhibitors. *Chem. Biodivers.* **2005**, *2*, 487–496. [[CrossRef](#)]
40. Seo, W.D.; Kim, J.H.; Kang, J.E.; Ryu, H.W.; Curtis-Long, M.J.; Lee, H.S.; Yang, M.S.; Park, K.H. Sulfonamide chalcone as a new class of alpha-glucosidase inhibitors. *Bioorg. Med. Chem. Lett.* **2005**, *15*, 5514–5516. [[CrossRef](#)]
41. Hasan, A.; Khan, K.M.; Sher, M.; Maharvi, G.M.; Nawaz, S.A.; Choudhary, M.I.; Atta ur, R.; Supuran, C.T. Synthesis and inhibitory potential towards acetylcholinesterase, butyrylcholinesterase and lipoxygenase of some variably substituted chalcones. *J. Enzym. Inhib. Med. Chem.* **2005**, *20*, 41–47. [[CrossRef](#)] [[PubMed](#)]
42. Najafian, M.; Ebrahim-Habibi, A.; Hezareh, N.; Yaghmaei, P.; Parivar, K.; Larijani, B. Trans-chalcone: A novel small molecule inhibitor of mammalian alpha-amylase. *Mol. Biol. Rep.* **2011**, *38*, 1617–1620. [[CrossRef](#)] [[PubMed](#)]
43. Kashani-Amin, E.; Larijani, B.; Ebrahim-Habibi, A. Neohesperidin dihydrochalcone: Presentation of a small molecule activator of mammalian alpha-amylase as an allosteric effector. *FEBS Lett.* **2013**, *587*, 652–658. [[CrossRef](#)] [[PubMed](#)]
44. Hofmann, E.; Webster, J.; Do, T.; Kline, R.; Snider, L.; Hauser, Q.; Higginbottom, G.; Campbell, A.; Ma, L.; Paula, S. Hydroxylated chalcones with dual properties: Xanthine oxidase inhibitors and radical scavengers. *Bioorg. Med. Chem.* **2016**, *24*, 578–587. [[CrossRef](#)]
45. Mathew, B.; Mathew, G.E.; Ucar, G.; Joy, M.; Nafna, E.K.; Suresh, J. Monoamine oxidase inhibitory activity of methoxy-substituted chalcones. *Int. J. Boil. Macromol.* **2017**, *104*, 1321–1329. [[CrossRef](#)]
46. Mathew, B.; Mathew, G.E.; Ucar, G.; Baysal, I.; Suresh, J.; Mathew, S.; Haridas, A.; Jayaprakash, V. Potent and Selective Monoamine Oxidase-B Inhibitory Activity: Fluoro- vs. Trifluoromethyl-4-hydroxylated Chalcone Derivatives. *Chem. Biodivers.* **2016**, *13*, 1046–1052. [[CrossRef](#)]

47. Minders, C.; Petzer, J.P.; Petzer, A.; Lourens, A.C. Monoamine oxidase inhibitory activities of heterocyclic chalcones. *Bioorg. Med. Chem. Lett.* **2015**, *25*, 5270–5276. [[CrossRef](#)]
48. Liu, H.R.; Liu, X.J.; Fan, H.Q.; Tang, J.J.; Gao, X.H.; Liu, W.K. Design, synthesis and pharmacological evaluation of chalcone derivatives as acetylcholinesterase inhibitors. *Bioorg. Med. Chem.* **2014**, *22*, 6124–6133. [[CrossRef](#)]
49. Liu, H.R.; Huang, X.Q.; Lou, D.H.; Liu, X.J.; Liu, W.K.; Wang, Q.A. Synthesis and acetylcholinesterase inhibitory activity of Mannich base derivatives flavokawain B. *Bioorg. Med. Chem. Lett.* **2014**, *24*, 4749–4753. [[CrossRef](#)]
50. Shah, M.S.; Khan, S.U.; Ejaz, S.A.; Afridi, S.; Rizvi, S.U.; Najam-Ul-Haq, M.; Iqbal, J. Cholinesterases inhibition and molecular modeling studies of piperidyl-thienyl and 2-pyrazoline derivatives of chalcones. *Biochem. Biophys. Res. Commun.* **2017**, *482*, 615–624. [[CrossRef](#)] [[PubMed](#)]
51. Bag, S.; Ghosh, S.; Tulsan, R.; Sood, A.; Zhou, W.; Schifone, C.; Foster, M.; LeVine, H., III; Torok, B.; Torok, M. Design, synthesis and biological activity of multifunctional alpha,beta-unsaturated carbonyl scaffolds for Alzheimer's disease. *Bioorg. Med. Chem. Lett.* **2013**, *23*, 2614–2618. [[CrossRef](#)] [[PubMed](#)]
52. Liu, H.; Fan, H.; Gao, X.; Huang, X.; Liu, X.; Liu, L.; Zhou, C.; Tang, J.; Wang, Q.; Liu, W. Design, synthesis and preliminary structure-activity relationship investigation of nitrogen-containing chalcone derivatives as acetylcholinesterase and butyrylcholinesterase inhibitors: A further study based on Flavokawain B Mannich base derivatives. *J. Enzym. Inhib. Med. Chem.* **2016**, *31*, 580–589. [[CrossRef](#)] [[PubMed](#)]
53. Kang, J.E.; Cho, J.K.; Curtis-Long, M.J.; Ryu, H.W.; Kim, J.H.; Kim, H.J.; Yuk, H.J.; Kim, D.W.; Park, K.H. Inhibitory evaluation of sulfonamide chalcones on β -secretase and acylcholinesterase. *Molecules* **2012**, *18*, 140–153. [[CrossRef](#)] [[PubMed](#)]
54. Ma, L.; Yang, Z.; Li, C.; Zhu, Z.; Shen, X.; Hu, L. Design, synthesis and SAR study of hydroxychalcone inhibitors of human beta-secretase (BACE1). *J. Enzym. Inhib. Med. Chem.* **2011**, *26*, 643–648. [[CrossRef](#)] [[PubMed](#)]
55. Wang, Z. *Comprehensive Organic Name Reactions and Reagents*; John Wiley & Sons: New York, NY, USA, 2010.
56. Balkrishna, A.; Pokhrel, S.; Tomer, M.; Verma, S.; Kumar, A.; Nain, P.; Gupta, A.; Varshney, A. Anti-Acetylcholinesterase Activities of Mono-Herbal Extracts and Exhibited Synergistic Effects of the Phytoconstituents: A Biochemical and Computational Study. *Molecules* **2019**, *24*, 4175. [[CrossRef](#)]
57. Paudel, P.; Seong, S.H.; Zhou, Y.; Ha, M.T.; Min, B.S.; Jung, H.A.; Choi, J.S. Arylbenzofurans from the Root Bark of *Morus alba* as Triple Inhibitors of Cholinesterase, β -Site Amyloid Precursor Protein Cleaving Enzyme 1, and Glycogen Synthase Kinase-3 β : Relevance to Alzheimer's Disease. *ACS Omega* **2019**, *4*, 6283–6294. [[CrossRef](#)]
58. Jannat, S.; Balupuri, A.; Hong, S.S.; Choi, C.; Choi, Y.-H.; Ku, J.-M.; Kim, W.; Leem, J.; Kim, J.; Shrestha, A.; et al. Inhibition of β -site amyloid precursor protein cleaving enzyme 1 and cholinesterases by pterosins via a specific structure–activity relationship with a strong BBB permeability. *Exp. Mol. Med.* **2019**, *51*. [[CrossRef](#)]
59. Sussman, J.L.; Silman, I. Acetylcholinesterase: Structure and use as a model for specific cation-protein interactions. *Curr. Opin. Struct. Biol.* **1992**, *2*, 721–729. [[CrossRef](#)]
60. ChEMBL Database. Available online: <https://www.ebi.ac.uk/chembl/> (accessed on 20 May 2019).
61. Beswick, P.; Charrier, N.; Clarke, B.; Demont, E.; Dingwall, C.; Dunsdon, R.; Faller, A.; Gleave, R.; Hawkins, J.; Hussain, I.; et al. BACE-1 inhibitors part 3: Identification of hydroxy ethylamines (HEAs) with nanomolar potency in cells. *Bioorg. Med. Chem. Lett.* **2008**, *18*, 1022–1026. [[CrossRef](#)]
62. Charrier, N.; Clarke, B.; Cutler, L.; Demont, E.; Dingwall, C.; Dunsdon, R.; Hawkins, J.; Howes, C.; Hubbard, J.; Hussain, I.; et al. Second generation of BACE-1 inhibitors. Part 1: The need for improved pharmacokinetics. *Bioorg. Med. Chem. Lett.* **2009**, *19*, 3664–3668. [[CrossRef](#)]
63. Charrier, N.; Clarke, B.; Cutler, L.; Demont, E.; Dingwall, C.; Dunsdon, R.; Hawkins, J.; Howes, C.; Hubbard, J.; Hussain, I.; et al. Second generation of BACE-1 inhibitors part 3: Towards non hydroxyethylamine transition state mimetics. *Bioorg. Med. Chem. Lett.* **2009**, *19*, 3674–3678. [[CrossRef](#)]
64. Chen, S.H.; Lamar, J.; Guo, D.; Kohn, T.; Yang, H.C.; McGee, J.; Timm, D.; Erickson, J.; Yip, Y.; May, P.; et al. P3 cap modified Phe*-Ala series BACE inhibitors. *Bioorg. Med. Chem. Lett.* **2004**, *14*, 245–250. [[CrossRef](#)] [[PubMed](#)]
65. Clarke, B.; Demont, E.; Dingwall, C.; Dunsdon, R.; Faller, A.; Hawkins, J.; Hussain, I.; MacPherson, D.; Maile, G.; Matico, R.; et al. BACE-1 inhibitors part 2: Identification of hydroxy ethylamines (HEAs) with reduced peptidic character. *Bioorg. Med. Chem. Lett.* **2008**, *18*, 1017–1021. [[CrossRef](#)]

66. Ginman, T.; Viklund, J.; Malmstrom, J.; Blid, J.; Emond, R.; Forsblom, R.; Johansson, A.; Kers, A.; Lake, F.; Sehgelmeble, F.; et al. Core refinement toward permeable beta-secretase (BACE-1) inhibitors with low hERG activity. *J. Med. Chem.* **2013**, *56*, 4181–4205. [[CrossRef](#)] [[PubMed](#)]
67. Hamada, Y.; Kiso, Y. Advances in the identification of beta-secretase inhibitors. *Expert Opin. Drug Discov.* **2013**, *8*, 709–731. [[CrossRef](#)] [[PubMed](#)]
68. Ng, R.A.; Sun, M.; Bowers, S.; Hom, R.K.; Probst, G.D.; John, V.; Fang, L.Y.; Maillard, M.; Gailunas, A.; Brogley, L.; et al. Design and synthesis of hydroxyethylamine (HEA) BACE-1 inhibitors: Prime side chromane-containing inhibitors. *Bioorg. Med. Chem. Lett.* **2013**, *23*, 4674–4679. [[CrossRef](#)]
69. Oehlrich, D.; Prokopcova, H.; Gijssen, H.J. The evolution of amidine-based brain penetrant BACE1 inhibitors. *Bioorg. Med. Chem. Lett.* **2014**, *24*, 2033–2045. [[CrossRef](#)]
70. Weiss, M.M.; Williamson, T.; Babu-Khan, S.; Bartberger, M.D.; Brown, J.; Chen, K.; Cheng, Y.; Citron, M.; Croghan, M.D.; Dineen, T.A.; et al. Design and preparation of a potent series of hydroxyethylamine containing beta-secretase inhibitors that demonstrate robust reduction of central beta-amyloid. *J. Med. Chem.* **2012**, *55*, 9009–9024. [[CrossRef](#)]
71. Woltering, T.J.; Wostl, W.; Hilpert, H.; Rogers-Evans, M.; Pinard, E.; Mayweg, A.; Gobel, M.; Banner, D.W.; Benz, J.; Travagli, M.; et al. BACE1 inhibitors: A head group scan on a series of amides. *Bioorg. Med. Chem. Lett.* **2013**, *23*, 4239–4243. [[CrossRef](#)]
72. Charrier, N.; Clarke, B.; Demont, E.; Dingwall, C.; Dunsdon, R.; Hawkins, J.; Hubbard, J.; Hussain, I.; Maile, G.; Matico, R.; et al. Second generation of BACE-1 inhibitors, Part 2: Optimisation of the non-prime side substituent. *Bioorg. Med. Chem. Lett.* **2009**, *19*, 3669–3673. [[CrossRef](#)] [[PubMed](#)]
73. Gómez-Jiménez, G.; Gonzalez-Ponce, K.; Castillo-Pazos, D.J.; Madariaga-Mazon, A.; Barroso-Flores, J.; Cortes-Guzman, F.; Martinez-Mayorga, K. The OECD Principles for (Q)SAR Models in the Context of Knowledge Discovery in Databases (KDD). *Adv. Protein Chem. Struct. Biol.* **2018**, *113*, 85–117. [[CrossRef](#)] [[PubMed](#)]
74. Ojha, P.K.; Mitra, I.; Das, R.N.; Roy, K. Further exploring rm2 metrics for validation of QSPR models. *Chemom. Intell. Lab. Syst.* **2011**, *107*, 194–205. [[CrossRef](#)]
75. Thai, K.-M.; Bui, Q.-H.; Tran, T.-D.; Huynh, T.-N.-P. QSAR modeling on benzo[c]phenanthridine analogues as topoisomerase I inhibitors and anti-cancer agents. *Molecules* **2012**, *17*, 5690–5712. [[CrossRef](#)] [[PubMed](#)]
76. Chirico, N.; Gramatica, P. Real external predictivity of QSAR models: How to evaluate it? Comparison of different validation criteria and proposal of using the concordance correlation coefficient. *J. Chem. Inf. Model.* **2011**, *51*, 2320–2335. [[CrossRef](#)] [[PubMed](#)]
77. Roy, K.; Ambure, P.; Kar, S. How Precise Are Our Quantitative Structure–Activity Relationship Derived Predictions for New Query Chemicals? *ACS Omega* **2018**, *3*, 11392–11406. [[CrossRef](#)] [[PubMed](#)]
78. Niraj, R.R.; Saini, V.; Kumar, A. QSAR analyses of organophosphates for insecticidal activity and its in-silico validation using molecular docking study. *Environ. Toxicol. Pharmacol.* **2015**, *40*, 886–894. [[CrossRef](#)]
79. Ambure, P.; Roy, K. Understanding the structural requirements of cyclic sulfone hydroxyethylamines as hBACE1 inhibitors against A β plaques in Alzheimer’s disease: A predictive QSAR approach. *RSC Adv.* **2016**, *6*, 28171–28186. [[CrossRef](#)]
80. Hossain, T.; Islam, M.A.; Pal, R.; Saha, A. Exploring structural requirement and binding interactions of β -amyloid cleavage enzyme inhibitors using molecular modeling techniques. *Med. Chem. Res.* **2013**, *22*, 4766–4774. [[CrossRef](#)]
81. Tran, T.-D.N.; Nguyen, V.; Nguyen, N.-S.; Nguyen, D.-M.; Nguyen, T.-T.-H.; Le, M.-T.; Thai, K.-M. Synthesis of Novel Chalcones as Acetylcholinesterase Inhibitors. *Appl. Sci.* **2016**, *6*, 198. [[CrossRef](#)]
82. Nuthakki, V.K.; Sharma, A.; Kumar, A.; Bharate, S.B. Identification of embelin, a 3-undecyl-1,4-benzoquinone from *Embelia ribes* as a multitargeted anti-Alzheimer agent. *Drug Dev. Res.* **2019**, *80*, 655–665. [[CrossRef](#)]
83. Olasehinde, T.A.; Mabinya, L.V.; Olaniran, A.O.; Okoh, A.I. Chemical characterization, antioxidant properties, cholinesterase inhibitory and anti-amyloidogenic activities of sulfated polysaccharides from some seaweeds. *Bioact. Carbohydr. Diet. Fibre* **2019**, *18*, 100182. [[CrossRef](#)]
84. Chemical Computing Group. MOE 2008.10 edition. Available online: <https://www.chemcomp.com/> (accessed on 20 May 2019).
85. Sybyl X 2.0. Available online: <https://sybyl-x.software.informer.com/2.0/> (accessed on 20 May 2019).
86. Demel, M.; Janecek, A.; Thai, K.-M.; Ecker, G.; Gansterer, W. Predictive QSAR Models for Polyspecific Drug Targets: The Importance of Feature Selection. *Curr. Comput. Aided Drug Des.* **2008**, *4*, 91–110. [[CrossRef](#)]

87. RapidMiner 5.3.013. Available online: <https://rapidminer.com/> (accessed on 20 May 2019).
88. Weka Software 3.8. Available online: <https://waikato.github.io/weka-wiki/> (accessed on 20 May 2019).
89. Ngo, T.D.; Tran, T.D.; Le, M.T.; Thai, K.M. Computational predictive models for P-glycoprotein inhibition of in-house chalcone derivatives and drug-bank compounds. *Mol. Divers.* **2016**, *20*, 945–961. [[CrossRef](#)] [[PubMed](#)]
90. Azam, F.; Madi, A.M.; Ali, H.I. Molecular Docking and Prediction of Pharmacokinetic Properties of Dual Mechanism Drugs that Block MAO-B and Adenosine A(2A) Receptors for the Treatment of Parkinson's Disease. *J. Young Pharm.* **2012**, *4*, 184–192. [[CrossRef](#)]
91. Protein Data Bank. Available online: <https://www.rcsb.org/> (accessed on 20 May 2019).
92. LeadIT 2.0.2. Available online: <https://www.biosolveit.de/LeadIT/> (accessed on 20 May 2019).
93. Kitchen, D.B.; Decornez, H.; Furr, J.R.; Bajorath, J. Docking and scoring in virtual screening for drug discovery: Methods and applications. *Nat. Rev. Drug Discov.* **2004**, *3*, 935–949. [[CrossRef](#)]
94. Pagadala, N.S.; Syed, K.; Tuszynski, J. Software for molecular docking: A review. *Biophys. Rev.* **2017**, *9*, 91–102. [[CrossRef](#)]

Sample Availability: Samples of the compounds are not available from the authors.



© 2020 by the authors. Licensee MDPI, Basel, Switzerland. This article is an open access article distributed under the terms and conditions of the Creative Commons Attribution (CC BY) license (<http://creativecommons.org/licenses/by/4.0/>).